AD-A090 633 AIR FORCE INST OF TECH WRIGHT-PATTERSON AFB OH F/G 4/2
A STUDY OF THE VERTICAL DISTRIBUTION OF OZONE AND THE VARIABILI--ETC(U)
1979 D R HOOD
UNCLASSIFIED AFIT-CI-79-160T NL

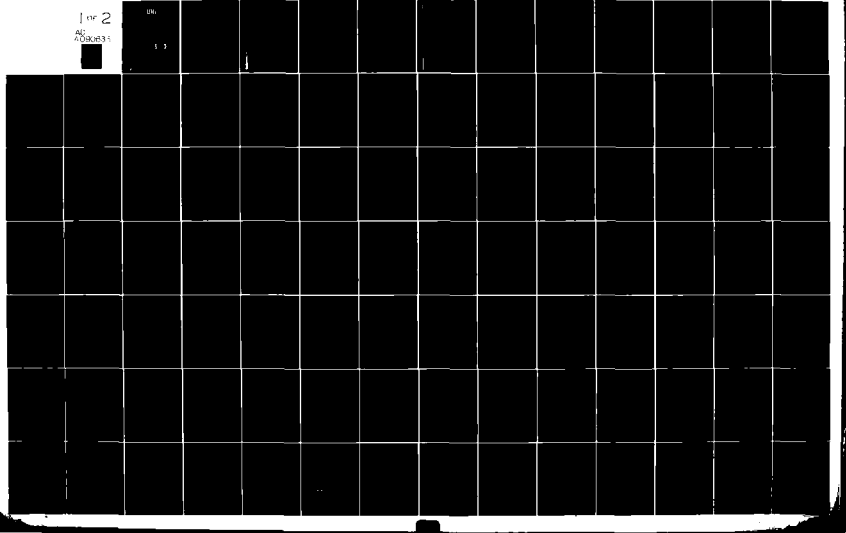

LEVEL II

UNCLASS

SECURITY CLASSIFICATION OF THIS PAGE (When Data Entered)

| REPORT DOCUMENTATION PAGE | READ INSTRUCTIONS BEFORE COMPLETING FORM |
|---|---|
| 1. REPORT NUMBER: AFIT/CI-79-160T | 2. GOVT ACCESSION NO.: AD-A090 633 |
| 3. RECIPIENT'S CATALOG NUMBER: Master's Thesis | |
| 4. TITLE (and Subtitle): A Study of the Vertical Distribution of Ozone and the Variability of the Wind Field Above a Nocturnal Radiation Inversion | 5. TYPE OF REPORT & PERIOD COVERED: Thesis |
| | 6. PERFORMING ORG. REPORT NUMBER |
| 7. AUTHOR(s): Capt Donald Rogers Hood | 8. CONTRACT OR GRANT NUMBER(s) |
| 9. PERFORMING ORGANIZATION NAME AND ADDRESS: Students address: AFIT Student at: North Carolina State University | 10. PROGRAM ELEMENT, PROJECT, TASK AREA & WORK UNIT NUMBERS |
| 11. CONTROLLING OFFICE NAME AND ADDRESS: AFIT/NR, WPAFB OH 45433 | 12. REPORT DATE: 1979 |
| | 13. NUMBER OF PAGES: 92 |
| 14. MONITORING AGENCY NAME & ADDRESS (if different from Controlling Office): 12 101 | 15. SECURITY CLASS. (of this report): UNCLASS |
| | 15a. DECLASSIFICATION/DOWNGRADING SCHEDULE |

16. DISTRIBUTION STATEMENT (of this Report)

Approved for Public Release, Distribution Unlimited

17. DISTRIBUTION STATEMENT (of the abstract entered in Block 20, if different from Report)

APPROVED FOR PUBLIC RELEASE AFR 190-17.

Fredric C. Lynch

FREDRIC C. LYNCH, Major, USAF
Director of Public Affairs

23 SEP 1980

18. SUPPLEMENTARY NOTES

Approved for public release: IAW AFR 190-17

Air Force Institute of Technology (ATC)
Wright-Patterson AFB, OH 45433

19. KEY WORDS (Continue on reverse side if necessary and identify by block number)

20. ABSTRACT (Continue on reverse side if necessary and identify by block number)

SEE ATTACHED ABSTRACT

DD FORM 1 JAN 73 1473 EDITION OF 1 NOV 65 IS OBSOLETE

012200

UNCLASS

SECURITY CLASSIFICATION OF THIS PAGE (When Data Entered)

79-160T

# A STUDY OF THE VERTICAL DISTRIBUTION OF OZONE AND THE VARIABILITY OF THE WIND FIELD ABOVE A NOCTURNAL RADIATION INVERSION

by

DONALD ROGERS HOOD

A thesis submitted to the Graduate Faculty of
North Carolina State University
in partial fulfillment of the
requirements for the Degree of
Master of Science

METEOROLOGY



Raleigh

1 9 7 9

APPROVED BY:

Chairman of Advisory Committee

ABSTRACT

~~HOOD, DONALD ROGERS.~~ A Study of the Vertical Distribution of Ozone and the Variability of the Wind Field Above a Nocturnal Radiation Inversion. (Under the direction of Allen J. Riordan.)

The vertical distribution of ozone prior to the morning breakdown of the radiation inversion is related to the changes in the nocturnal wind field and the trajectory of the layer containing the ozone. Helicopter and hourly pilot-balloon data collected on five days during August 1976, in St. Louis, Missouri, were analyzed.

The ozone was assumed to be uniformly mixed throughout the boundary layer at sunset the previous evening. The study indicates that the similarities and differences between the vertical distribution of ozone assumed at sunset and observed the following morning are related to the variability of the nocturnal wind field.

Analysis of height-time cross sections of the nocturnal wind field indicated that the winds exhibited both vertical and temporal variability above an observation point. Most of the temporal variability in the nocturnal wind field occurs between scheduled radiosonde launch times and will not be completely detected. Therefore, the trajectory computations will not entirely represent the changes which occur. The study also indicates that due to the vertical variability of the wind field, more representative trajectories can be obtained by computing the trajectories for several thin layers versus computing a single trajectory for a thick layer.

Donald Rogers Hood

A Study Of The Vertical Distribution Of Ozone
And The Variability Of The Wind Field Above
A Nocturnal Radiation Inversion

Capt. , USAF

1979

92

Master Of Science, Meteorology

North Carolina State University

# BIOGRAPHY

Donald Rogers Hood was born in Calhoun, Georgia, on June 19, 1947. He received his elementary and secondary education in Calhoun, graduating from Calhoun High School in 1965. In 1969 the author received a Bachelor of Science degree with a major in Physics from Berry College, Mt. Berry, Georgia. In 1977 he received a Master of Business Administration degree from the University of Utah.

After receiving his commission as a second lieutenant in the United States Air Force in October 1970, he was stationed at Columbus Air Force Base, Mississippi; North Carolina State University, Raleigh, North Carolina; Seymour-Johnson Air Force Base, North Carolina; and RAF Mildenhall, England. The author returned to North Carolina State University in January 1978, to undertake a course of study leading to the Master of Science degree in Meteorology.

The author is married to the former Miss Shelia Smith and has three children, Ashlie Camille, Jason Patrick and Jeffrey Michael.

# ACKNOWLEDGEMENTS

The author would like to express his appreciation to everyone who contributed to the completion of this thesis. The advice and guidance of Dr. Allen Riordan, Chairman of the Advisory Committee, have been invaluable in the completion of this study. A special thanks is extended to Mr. Roy Evans of the Environmental Protection Agency who furnished data and aided in the completion of the research. Gratitude is also expressed to the other members of the Advisory Committee for their assistance and suggestions: Dr. Walter Saucier and Dr. Charles E. Anderson.

Finally, the author wishes to thank his wife, Shelia, and his children for their patience and sacrifice during the course of this study.

TABLE OF CONTENTS

TABLE OF CONTENTS (Continued)

# 1.0 INTRODUCTION

The formation, destruction, and transport of ozone can be investigated through examination of air pollution and meteorological parameters measured in St. Louis, Missouri, as part of the Regional Air Pollution Study (RAPS). RAPS was a multi-year research program conducted by the Environmental Protection Agency (EPA) in St. Louis, in which air quality and meteorological parameters were measured both at the surface and in the lower troposphere from 1974 through 1976. As part of the RAPS, a network of air monitoring stations, called the Regional Air Monitoring System (RAMS), was established to provide a large body of ground level air monitoring data (Figure 1.1). Figure 1.1 also depicts four upper air network sites (UAN) numbered 141, 142, 143, and 144, whose purpose was to provide upper air wind data using pilot-balloons (PIBALs) and radiosondes. In addition, during data-intensive periods, helicopter flights originating at Smartt Field (Figure 1.1) were used to obtain the vertical distribution of ozone, total oxides of nitrogen, carbon monoxide, sulfur dioxide, particulate light scattering, temperature and dewpoint as a function of time and altitude. Also during data intensive periods PIBALs were launched each hour from all four UAN sites, with the exception of 0400, 1000, 1600, and 2200 CST, at which times radiosondes were launched from all four UAN sites.

The case studies to follow will use data collected during the summer 1976 data intensive period. The helicopter spirals used in the case studies were observed over Smartt Field which is located in a rural setting approximately 35 km north-northwest of the center of

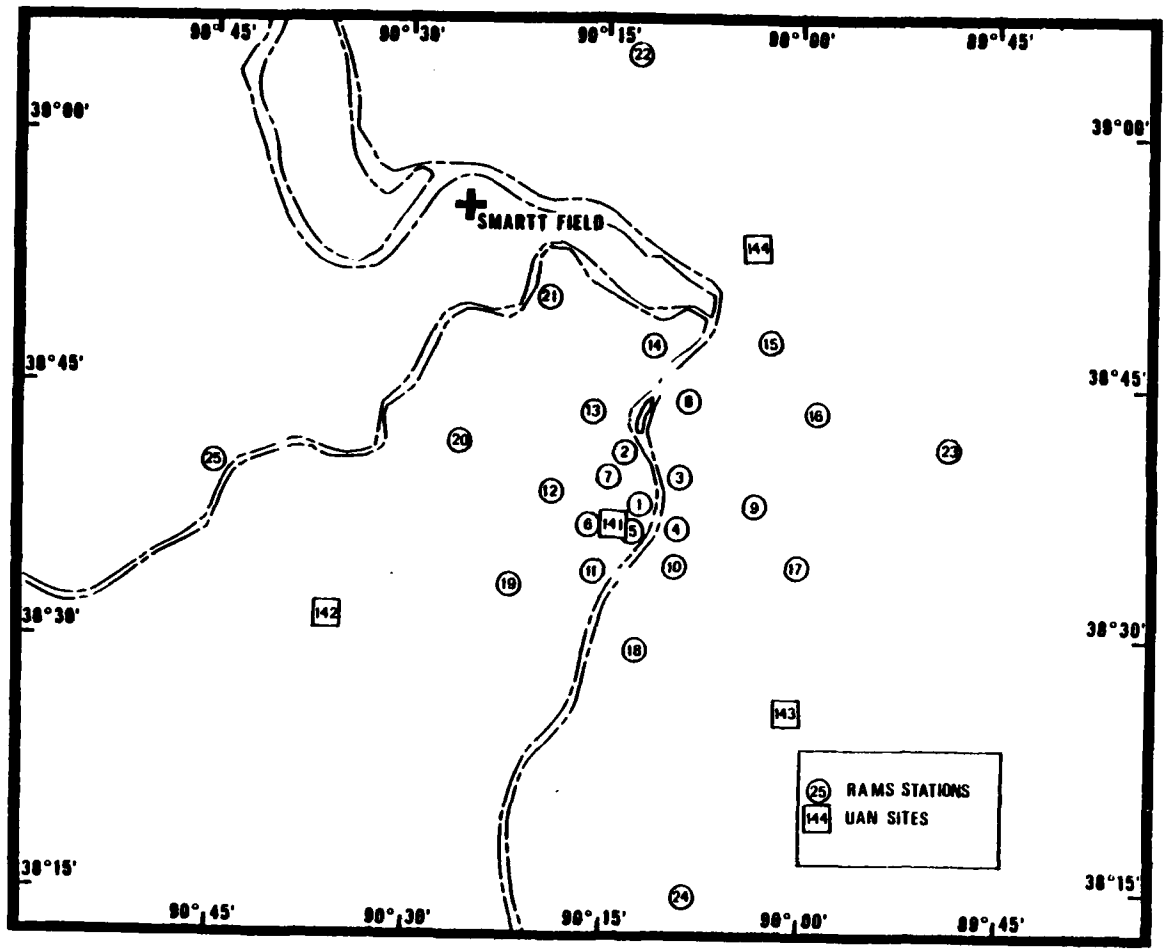


Figure 1.1 Map depicting RAPS facilities in St. Louis, Missouri

St. Louis. The case studies will also use PIBAL observations taken at UAN site 144 which is located approximately 25 km to the east-southeast of Smartt Field.

## 2.0 PURPOSE OF STUDY

The purpose of this study is to describe the early morning vertical distribution of ozone (the ozone profile) above Smartt Field and to relate the shape of the ozone profile to the changes in the wind field that have occurred since sunset on the previous evening and to the trajectory of the air containing the ozone prior to its arrival over Smartt Field.

# 3.0 REVIEW OF LITERATURE

## 3.1 Production of Ozone

The photochemical production of ozone near the earth's surface is usually attributed to the nitrogen dioxide photolytic cycle. Nitrogen dioxide is highly reactive photochemically. The nitrogen dioxide photolytic cycle may be represented by

$$NO_2 + h\nu \rightarrow NO + O \quad (a)$$

$$O + O_2 + M \rightarrow O_3 + M \quad (b)$$

$$O_3 + NO \rightarrow NO_2 + O_2 \quad (c)$$

The initial $NO_2$ for reaction (a) is formed by the direct but slow oxidation of NO to $NO_2$. The combination of the above three reactions would tend to maintain at steady state a constant and low level of ozone (Wark and Warner, 1976).

If hydrocarbons are present, it is postulated that oxygen atoms attack various hydrocarbons. The oxidized compounds and free radicals then react with NO to form more $NO_2$. Since a significant portion of the NO now reacts with hydrocarbon species, less is available for reaction with $O_3$. This upsets the consumption of $O_3$ by NO, so that the $O_3$ level increases. Under the same circumstances, the $NO_2$ level also increases, rather than remaining relatively constant, since an additional source of $NO_2$ formation is present (Wark and Warner, 1976).

Singh et al. (1978) analyzed long-term ozone data collected at remote sites in Washington, Montana, Utah, Colorado, Hawaii and in

Germany. The long-term ozone data collected at the remote sites is complemented by aircraft data collected over the midwestern and northeastern United States to support the conclusion that a significant reservoir (maximum of 80 ppb in the spring to 40 ppb in the fall) of ozone is present in the troposphere. Only aircraft data were used for which the flight altitude was above the mixed layer within the free troposphere. The tropospheric ozone represents the background levels (typically 30 to 50 ppb in the month of August) observed in vertical ozone profiles. According to Singh et al., the diurnal variation of the background levels can be significantly affected by the transport of ozone from urban locations and by the presence of the oxides of nitrogen, either from natural or anthropogenic sources.

### 3.2 Destruction of Ozone

Harrison et al. (1978) discussed the nocturnal depletion of ozone in the urban and rural boundary layer. In urban areas the ozone depletion commences rapidly upon formation of the nocturnal stable layer. The ozone depletion is due to the injection of fresh primary pollutants, nitric oxide from the evening rush hour, being the most important. These primary pollutants react with ozone removing it from the atmosphere. The nocturnal stable layer and the lack of photolytic reactions prevent the replacement of the ozone from above. In rural areas the nocturnal depletion of ozone is due predominantly to dry deposition at the ground. The convectively stable layers produced by nocturnal surface cooling show marked variations in their ability to inhibit downward transport of ozone, thus allowing substantial variations in the depletion of ozone by dry deposition at the surface.

Galbally (1971) concludes that ozone destruction is proportional to the ozone concentration near the Earth's surface and it is consistent with the observations that this destruction takes place on the soil and vegetation surfaces. The ozone destruction coefficient (deposition velocity), determined over dry soil with clumps of dry grass and decaying vegetation in Australia, has an approximate value of 1 cm $s^{-1}$. Not all authors agree upon the appropriate value or values to be used for the dry deposition velocity. Garland and Derwent (1979) deduced deposition rates for ozone from profiles of concentration, wind speed and temperature measured over grassland in southern England. The mean deposition velocity was 0.58 cm $s^{-1}$ by day and 0.29 cm $s^{-1}$ by night.

Garland and Derwent (1979) also conclude that current knowledge of the nocturnal boundary layer is not sufficient to demonstrate beyond doubt that when the nocturnal decline of ozone occurs that it is due entirely to surface destruction, but it seems probable that this is the major cause.

Not all authors agree on which mechanism is most important for destruction of ozone, especially in rural areas. Ripperton and Vukovich (1971) state that theoretical considerations and field observations suggest that gas phase reactions are also a major sink for ozone. Their measurements, taken at Research Triangle Park, North Carolina, of the oxides of nitrogen and ozone and the simultaneous changes observed in their concentrations bear out the concept that the $NO_x$-$O_3$ reactions are a significant sink for ozone. Vukovich (1973), in presenting the results of follow-up work on the behavior of ozone in a rural boundary

layer, states that at night ozone destructive agents have a surface source and that gas phase destruction is a more important removal mechanism for ozone than destruction at the surface of the earth.

Despite the destruction which takes place below the stable layer, observations by Harrison et al. (1978), Galbally (1968), Ludwig (1979a, b) and Singh et al. (1978), indicate that the concentration of ozone above the stable layer is reduced little from the daytime peak.

## 3.3 Vertical Mixing of Ozone

The three-dimensional distribution of ozone in the atmosphere is not only governed by the chemical processes that lead to ozone formation and destruction, but it is also governed by the meteorological processes that enhance or inhibit mixing. Atmospheric mixing determines the depth to which the precursors of photochemical ozone are mixed while the ozone forms. Atmospheric mixing governs the amount of ozone that may be mixed downward to replace ozone destroyed at the surface (Ludwig, 1979a).

Ludwig (1979a) discusses six basic types of ozone profiles that are commonly observed. Most vertical profiles of ozone result from various combinations of chemical and meteorological processes and fall into the following limited categories as described by Ludwig (1979a). Figure 3.1 is a schematic representation of the six basic types of ozone profiles. The height and concentration scales that are used in the diagram are illustrative only. The sample values are generally typical, but observed conditions can differ from them substantially.

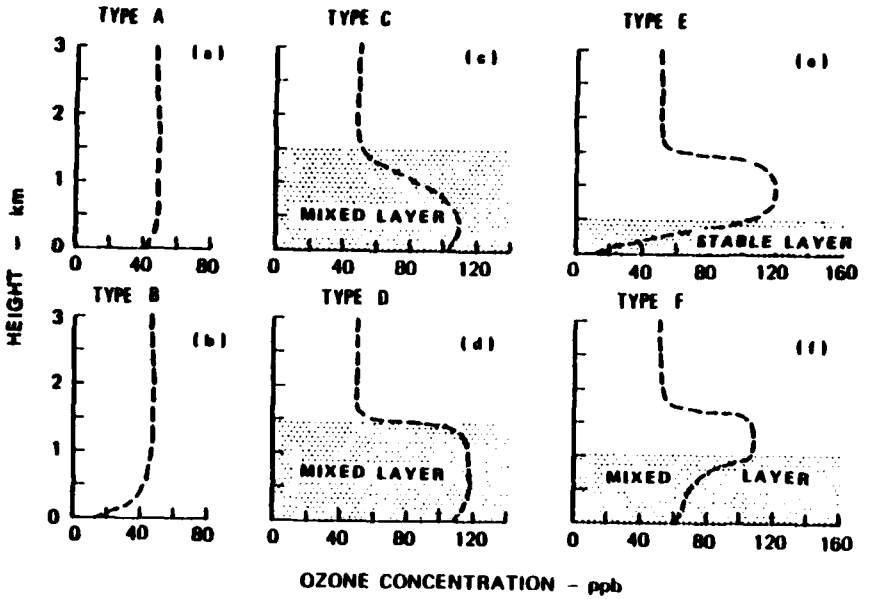


Figure 3.1 Six types of vertical profiles of ozone (after Ludwig, 1979a)

Figure 3.1a shows conditions that might prevail in a well-mixed air mass. Concentrations are nearly uniform with height, with a small decrease near the surface reflecting the destructive processes.

Figure 3.1b illustrates how the profile tends to be altered when a stable layer is formed at the surface. Under such conditions the ozone that is destroyed at the surface cannot be replaced by downward mixing from above, and hence, the steep gradient in the lowest layers develops. The stable layer at the surface can be formed by nighttime cooling or by passage of the air mass over a cooler surface such as a body of water during daylight hours.

Ludwig (1979a) describes Figure 3.1c as a schematic diagram of one type of vertical ozone profile that results when ozone forms from precursor emissions that have been released near the surface in the recent past, and have not had time to be completely mixed throughout the boundary layer. Ludwig did not specify what is meant by "recent past" in the article. If, as Figure 3.1c indicates, the pollutants have been released into or formed in a mixed layer, then the pollutant would be mixed uniformly to the top of the mixed layer almost instantaneously. The profile would then assume the shape illustrated in Figure 3.1d, where the precursors and the ozone that has formed from them are mixed throughout the boundary layer.

If a stable layer forms near the surface, then a severe gradient of concentration can develop leading to the type of profile illustrated schematically in Figure 3.1e. Further evolution of the profile can take place as shown in Figure 3.1f if a new mixed layer begins to form at the surface, but does not penetrate to the height of the earlier

mixed layer that led to the formation of a profile of the type shown in Figure 3.1d. In such cases there can be an elevated layer of ozone aloft whose concentration can be smaller than, equal to, or larger than the concentration in the mixed layer below. The concentrations within the underlying mixed layer can arise either from the mixing of pre-existing ozone downward or the formation of ozone from newly emitted precursors.

## 3.4 Transport of Ozone

The transport of ozone must be considered in analyzing vertical profiles over a particular city. Transport determines where the air entering the city originated, and, indirectly, the pollutant burden that it is carrying as it enters the city. The origin of the air determines its pollutant burden since the air emitted from a rural area would not have the same pollutant burden as air emitted from an urban-industrial area. The wind speed determines the volume of air into which the emissions are mixed and hence their concentration. The wind speed also determines how far the air travels downwind of a city during the time the photochemical reactions producing ozone are operative. The consideration of transport is important to the interpretation of vertical pollutant profiles (Ludwig, 1979b).

In order to better understand the transport of ozone, studies using instrumented aircraft have been undertaken to characterize the urban plume of metropolitan St. Louis, Missouri.

White et al. (1977) in their study of the St. Louis urban plume encountered a plume of ozone concentrations well above background levels.

Ozone concentrations within this plume often exceeded 200 ppb, and concentrations in excess of 300 ppb were recorded. They also found that on most sampling days the midday ozone levels outside the urban plume lay in the range of 70 to 120 ppb, levels which are substantially above those associated with clean air. White et al. (1977) mapped the St. Louis urban plume as far downwind as 160 km from the St. Louis Arch. At this distance, where concentrations outside the plume were 70 ppb or less, concentrations in the center of the plume remained as high as 120 ppb. Between 125 and 160 km downwind there was no significant decay in the flow rate of ozone and no significant increase in the crosswind and vertical dimensions of the urban plume. The aircraft flew no farther along the plume even though the plume was believed to extend much farther downwind. The length and concentration of the urban plume suggest that just as St. Louis can contribute to the ozone background of cities far downwind, much of the ozone background of St. Louis itself may not be natural, but instead may be due to cities and industry far upwind of St. Louis.

Hester et al. (1977) in their study of the St. Louis urban plume concluded that by afternoon the primary pollutants NO and $SO_2$ were, in general, depleted by dilution, chemical reactions, and other removal mechanisms as the plume proceeded away from the city, while ozone readings reached their highest values well downwind of the city. For example, on July 18, 1975, at the point where a maximum concentration of ozone was observed (approximately 50 km downwind) the NO and $NO_x$ maximum concentrations were about one-half to one-third lower than morning levels and it was no longer possible to define distinct

boundaries for the parcel of air which had been seen in a morning flight along the same path. Thus, the secondary pollutants, which are formed as the urban plume moves away from the city, seem to be the most significant components of the plume by early afternoon (1300 to 1400 CST on July 18, 1975). Hester et al. (1977) also concluded that power plant plumes within the urban plume appeared to cause depletion of ozone in the area of impaction on the urban plume and that this depletion of ozone was observed up to 60 km from the power plant.

Chatfield and Rasmussen (1977) concluded that individual urban plumes frequently modify ozone concentrations in the lowest kilometer of the troposphere and that large plumes may travel 200 to 300 km before losing their character.

In addition, White et al. (1977) have shown that individual regions within a metropolitan complex can emit urban plumes which are distinguishable as opposed to the entire metropolitan region emitting one plume. In the case of St. Louis, the urban plume of downtown St. Louis (motor vehicles) and the plume from Wood River (chemical industry) were detected immediately downwind of the metropolitan area. The combined initial width of the two plumes was about 50 km. Wood River is approximately 30 km north-northeast of downtown St. Louis.

## 3.5 Trajectories

Hoecker (1977) has shown that the errors in layer-average trajectories in northerly flow are widely but evenly scattered about a zero-error line in contrast to the right biased, but minimally scattered errors in southerly flow. His data suggest that larger

layer-average trajectory errors and larger error scatter can be expected in northerly flow than in southerly flow.

# 4.0 MATERIAL AND METHODS

## 4.1 Helicopter Data

Two Sikorsky S-58 helicopters equipped to measure ozone, total oxides of nitrogen, carbon monoxide, sulfur dioxide, particulate light scattering, temperature and dewpoint as functions of time and altitude were used in the Regional Air Pollution Study. The case studies in this paper involve the use of the ozone, total oxides of nitrogen, and temperature data as a function of time and altitude.

Ozone concentrations were measured with a REM Model 612 monitor. The REM instrument detects $O_3$ by measuring the light emitted by the chemiluminescent reaction of $O_3$ with ethylene gas. The lowest level of sensitivity for the REM is 1 ppb (part per billion), and the lowest range of operation is 0 to 20 ppb (Mage et al.).

NO and $NO_2$ concentrations were both measured by Monitor Labs, Inc., Model 8440 analyzer (ML 8440). The ML 8440 is able to monitor NO and $NO_x$ simultaneously. It monitors NO by measuring the light from the chemiluminescent reaction of NO with $O_3$. $NO_x$ concentrations are monitored by catalytically reducing $NO_2$ to NO and then measuring the total NO. The ML 8440 operates on a lowest range of 0 to 100 ppb full-scale (Mage et al.).

The temperature was determined continuously with an EG&G Vapormate II using a Model CS137 thermometer-hydrometer probe. The air temperature is sensed with a thermister located in the direct path of the moving air. The temperature sensor operates within the range of -40° to +49°C, with a temperature accuracy of $\pm$0.8°C.

The profiles used in the study were those obtained from the helicopter flight nearest to sunrise (sunrise ranged from 0503 CST on day 215 to 0508 CST on day 221). The helicopter data and profiles were obtained from Mr. Roy Evans, Environmental Protection Agency, Research Triangle Park, North Carolina. Mr. Evans has edited the helicopter records in detail to remove or to flag questionable data.

In each of the cases it will be assumed that any photochemical reactions which may be taking place are not significant enough to alter the shape of the ozone profile. An example of the changes in an ozone profile from before sunrise to after sunrise is given in Figure 4.1a, b, and c. The first spiral over Smartt Airfield was made at 0448 CST, the second at 0606 CST and the third at 0729 CST; sunrise occurred at 0504 CST. In each of the profiles the sharp decrease in ozone concentration (down to the noise levels) is associated with $NO_x$ scavenging due to a power plant plume. Both plumes rise slowly during the early morning with the lowest plume being absorbed by the mixed layer by the time of the 0729 CST spiral. Despite the fact that almost three hours has elapsed since the first spiral, including almost 2.5 hours since sunrise, the ozone profile has retained almost the same shape.

## 4.2 Trajectories

### 4.2.1 Heffter-Taylor Trajectory Model

Backward-in-time trajectories were constructed using the Heffter-Taylor Trajectory Model (Heffter et al., 1975). The trajectory model uses observed winds from 0000Z and 1200Z radiosondes plus 0600Z and 1200Z pilot balloons (PIBALs) when available, to compute the trajectory.

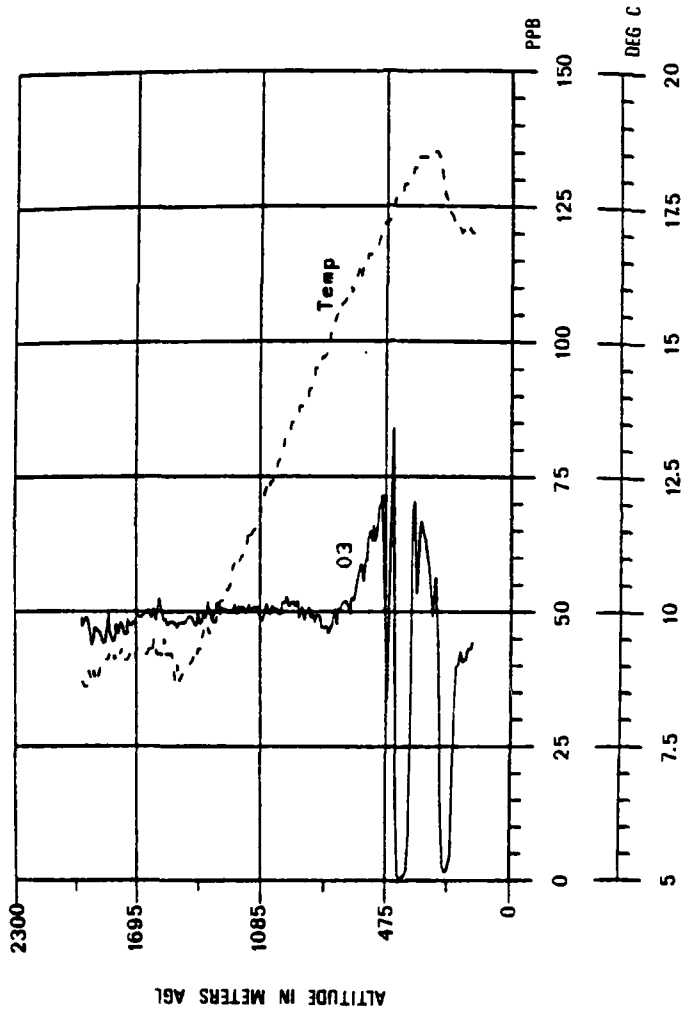


Figure 4.1a Ozone and temperature versus altitude, day 216. Downward spiral over Smartt Field between 0448 and 504 CST. NO and $NO_x$ data not available.

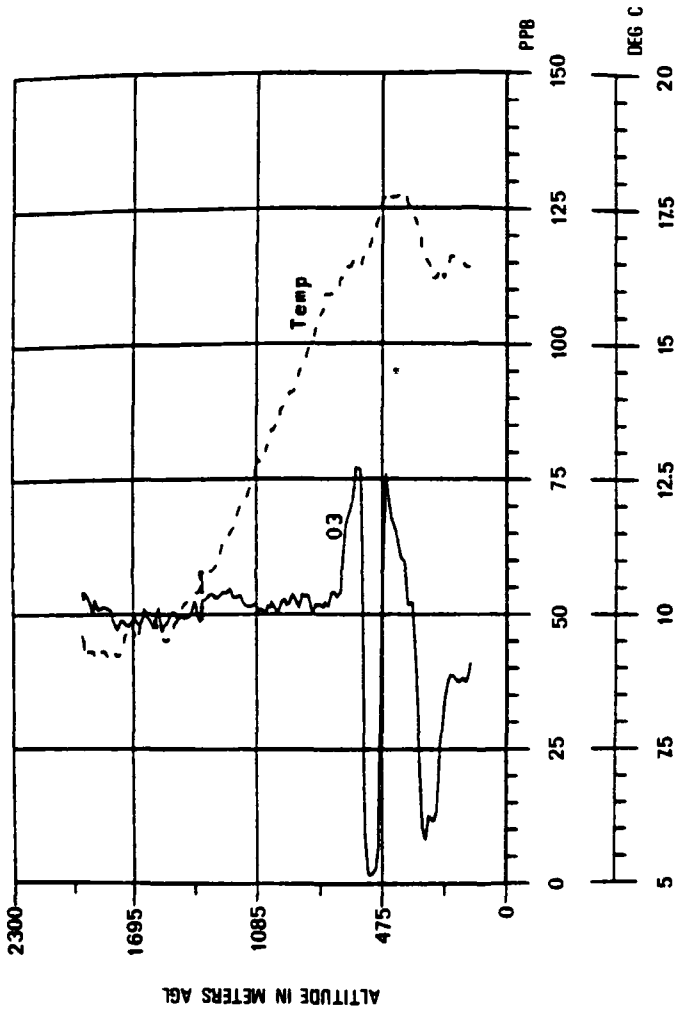


Figure 4.1b Ozone and temperature versus altitude, day 216. Upward spiral over Smartt Field between 0606 and 0617 CST. NO and $NO_x$ data not available.

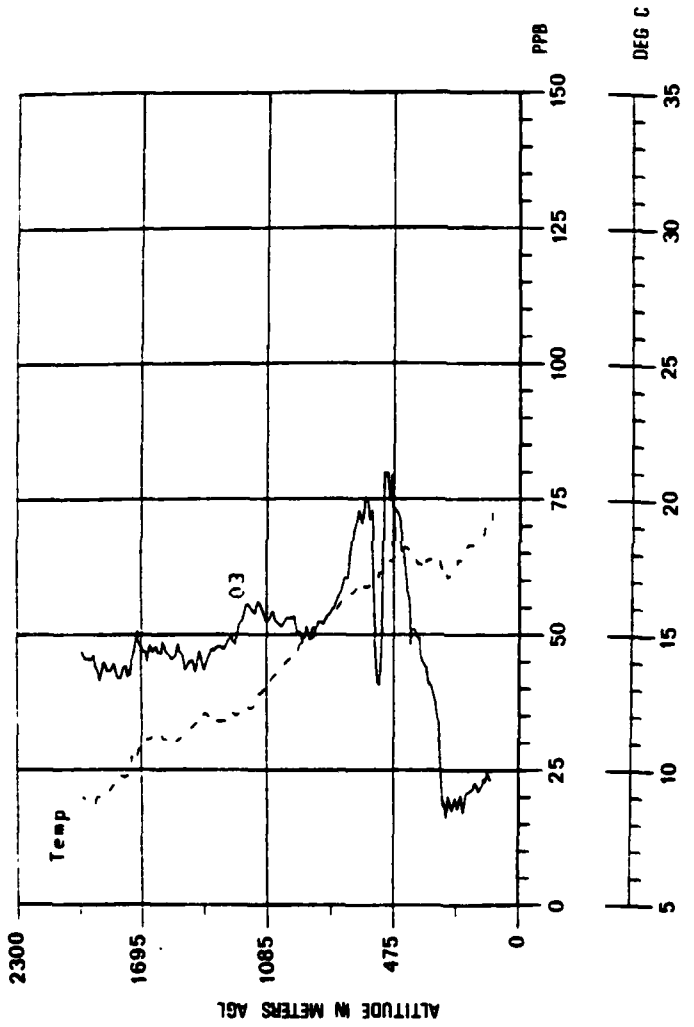


Figure 4.1c Ozone and temperature versus altitude, day 216. Upward spiral over Smartt Field between 0729 and 0743 CST. NO and $NO_x$ data not available.

A trajectory is composed of a series of 3-hour segments, each computed assuming persistence of the winds reported closest to the segment time. For example, the 3-hour segment 0000Z to 0300Z would assume the persistence of the 0000Z winds, while the 3-hour segment 0900Z to 1200Z would assume the backward persistence of the 1200Z winds.

The length of a 3-hour segment is determined using the average wind in the transport layer. The transport layer may be specified by the programmer or it may be computed using a modification, introduced by Heffter, to the Heffter-Taylor Trajectory Model (Conventry, 1979). The modification defines the top of the transport layer to be the height at which a significant inversion is present or a maximum level specified by the programmer, whichever is less. The inversion temperature difference is considered significant at 1°C per 200 meters. The base of the transport layer is determined by evaluating the vertical wind profile for significant shear. The maximum height of the layer base is set at 500 meters above average terrain by the program. The height of the layer base is determined by calculating the vertical wind shear (TW) between the two lowest reported levels (LVL and LVL-1) then testing to see if the shear is significant. Significant shear is defined as a TW greater than 5 meters per second ($m\,s^{-1}$). If the shear is not significant, then LVL is increased to the next reported level (thus also increasing the height of LVL-1) and TW is again computed. LVL is increased until TW is greater than 5 $m\,s^{-1}$ or the height of LVL exceeds 500 meters above average terrain height. When TW is greater than 5 $m\,s^{-1}$, then LVL becomes the base of the transport layer. When

LVL exceeds 500 meters above the average terrain height, then the base of the transport layer is set at 500 meters above the average terrain height.

Trajectories will be computed for each of the cases using the modification described above with the maximum top of the layer set at 2000 m. A set of three trajectories will also be computed with the base and the top of the transport layer being set by the programmer. The three trajectories will be for the following layers: 200 to 400, 900 to 1100, and 1700 to 1900 meters AGL.

The average wind in a layer is computed from the reported winds linearly weighted according to height (Fig. 4.2):

$$V_i = \frac{\sum^{\text{layer}} H_l V_l}{\sum^{\text{layer}} H_l}$$

where $V_i$ is the average wind in the layer at station i,

$V_l$ is a reported wind at level l, and

$H_l$ is a linear height weighting factor.

Each trajectory segment computed from observed winds ($TS_o$) is given by Figure 4.3:

$$TS_o = \frac{\sum^{R} DW_i AW_i TS_i}{\sum^{R} DW_i AW_i}$$

where:

$\sum^{R}$ indicates the summation over all winds within a radius R (300 nautical miles) of the segment origin;

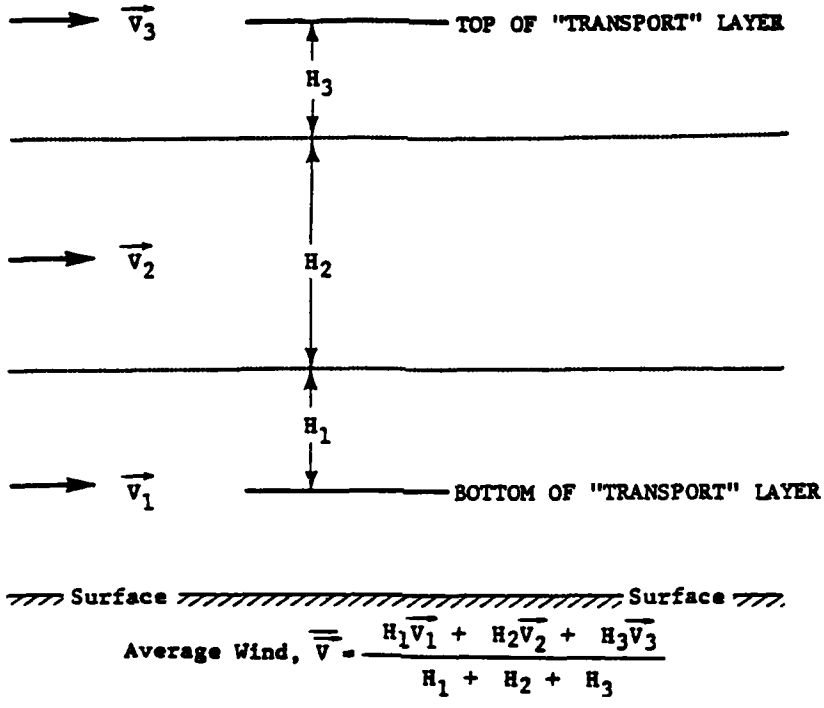


Figure 4.2 Scheme for determining an average wind in a layer (after Heffter et al., 1975).

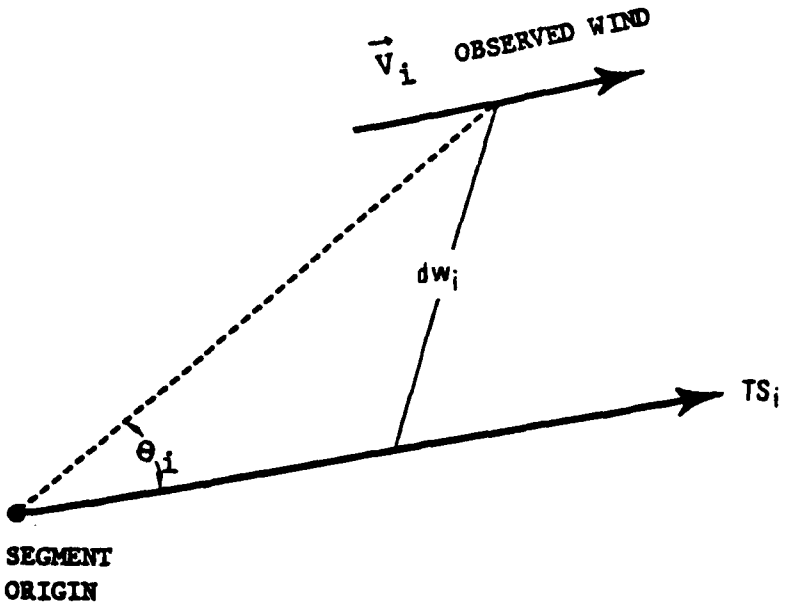


Figure 4.3 Configuration for determining a trajectory segment from observed winds (after Heffter et al., 1975).

$TS_i = (V_i)(\Delta t)$ is the contribution to the trajectory segment from an observed wind, $V_i$, and $\Delta t$ is the segment time interval (3 hours);

$DW_i = 1/dw_i^2$, the distance weighting factor, where $dw_i$ is the distance from an observed wind to the mid-point of $TS_i$ (the closest observations receive the greatest weight);

$AW_i = 1 - 0.5 \sin \Theta_i$, the alignment weighting factor, where $\Theta_i$ is the angle formed between $TS_i$ and a line drawn from the segment origin to a wind observation point (observations upwind and downwind receive the greatest weight).

### 4.2.2 Hand Computed Trajectory

Hourly PIBAL observations from site 144 were used to compute one hour trajectory segments for the layer from 200 to 400 m AGL. These winds were assumed to be representative over the area traversed by the trajectory. The trajectories originated in St. Louis at 0600 CST and were computed in one-hour segments (backward-in-time) until 1800 CST.

The wind data for site 144 were obtained from the Environmental Protection Agency, Research Triangle Park, North Carolina. The data received had been smoothed and interpolated to 50 meter AGL intervals.

The trajectories were computed using the following steps. First, an average wind was computed for each hour in the 200 m to 400 m layer. This layer-average wind was then averaged with the layer-average wind from the preceding hour (i.e., 0600 and 0500 CST winds are averaged). This average wind is then used to compute the trajectory segment.

## 4.3 Radiosonde and PIBAL Observations

Radiosonde and PIBAL observations were made in accordance with the appropriate Federal Meteorological Handbook.

Radiosonde and PIBAL observations were made at Sites 141, 142, 143, and 144 (Figure 1.1). In the case studies to follow upper level winds are obtained from site 144. The radiosondes were launched every 6 hours beginning at approximately 0400 CST. PIBALS were launched every hour, except on the hours when radiosondes were launched. The PIBAL data were obtained from the Environmental Protection Agency, Research Triangle Park, North Carolina. The data received from the EPA had been smoothed and interpolated to 50 m AGL intervals from the surface to 1300 m to 1800 m AGL, depending on the maximum height reported by the PIBAL.

# 5.0 CASE STUDIES

Five case studies detailing the changes in the wind field above a nocturnal radiation inversion and the effect of these changes on the shape of an early morning ozone profile are presented.

The five days were chosen based on the following criteria:

(1) Either a surface-based radiation inversion or a low level elevated inversion were present at the time of the helicopter spiral so that the profile was protected from scavenging from below.

(2) No frontal system was present in the St. Louis area from sunset the previous evening to the time of the helicopter spiral.

(3) The helicopter spiral was high enough to detect the subsidence inversion above Smartt Airfield. Thus, the changes in the wind field between the top of the radiation inversion and the base of the subsidence inversion can be related to the shape of the ozone profile.

(4) The helicopter spiral occurred within 3 hours after sunrise so that changes in the shape of the profile due to photochemical activity will be at a minimum.

Using the above criteria the 2nd, 3rd, 4th, 7th, and 8th of August 1976 were chosen from a total of eleven days with morning helicopter spirals for which edited helicopter data were available. Throughout the case studies these five days will be referred to as day 215, 216, 217, 220, and 221, respectively.

The case studies to follow will attempt to use the production, destruction, vertical mixing, and transport processes to explain the shape of the vertical profiles of ozone observed above Smartt Field on

the helicopter flight nearest to sunrise. The shape of the ozone profile at sunset on the previous evening will be assumed to be a Type D profile (Figure 3.2d) as described by Ludwig (1979a). The changes which take place below the radiation inversion will be assumed to have been caused by destructive processes while it will be assumed that the changes above the radiation inversion are due to transport processes. Since the changes in the ozone profile to be examined take place after sunset, it will be assumed that no ozone production is taking place in the lower troposphere.

The case studies to follow will also illustrate the variability in wind speed and direction between 1800 CST and 0800 CST in the layer between the top of the radiation inversion and the base of the subsidence inversion. This variability in wind speed and direction will then be related to changes in the shape of the ozone profile.

## 5.1 Case I: Day 215

### 5.1.1 Synoptic Chart Discussion

The surface analysis for 0600 CST on day 215 (Figure 5.1) indicated that a high pressure center was located over North Dakota, with an associated ridge extending eastward to the east coast and as far south as Tennessee, Louisiana, and Texas. The cold front near the Gulf of Mexico had passed through St. Louis at approximately 1300 CST on 31 July (day 213).

At 0600 CST on day 215 the 850 mb high was located over Northern North Dakota with an associated ridge covering the central United States to the Gulf Coast of Louisiana and Texas. The height field at 700 mb differs but little from that at 850 mb.

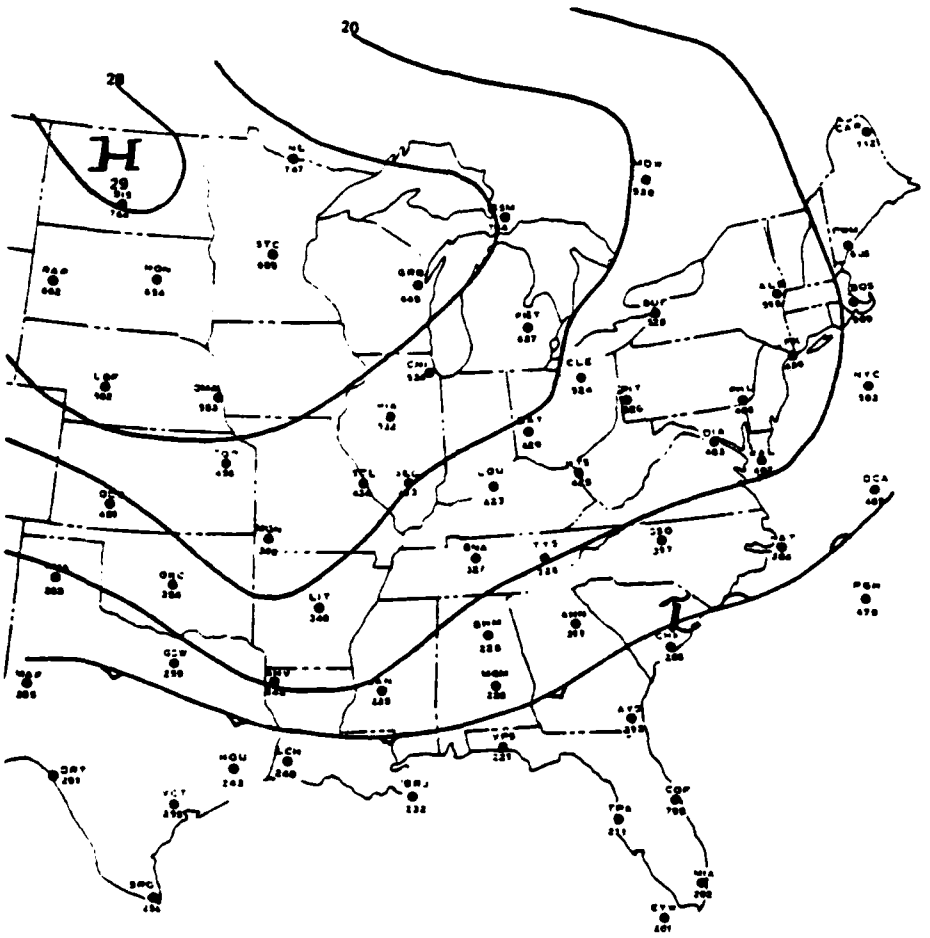


Figure 5.1 Surface analysis for day 215 at 0600 CST.

The high pressure center to the north-northwest of Missouri is causing a north-northeast flow into the St. Louis area at the surface and at 850 mb. The trough extending out of Canada is causing a northwesterly flow over eastern Missouri at 700 mb.

### 5.1.2 Trajectory Analysis

The layer-average wind trajectory for day 215 is shown in Figure 5.2. The trajectory begins in southern Canada to the north of Lake Superior, moves south along western Lake Michigan passing near Milwaukee and Chicago then turns southwest to St. Louis. The total length of the trajectory was approximately 1500 km.

The 12-hour trajectory segments for day 215 are nearly uniform in length due to the persistent north-northeasterly flow ahead of the advancing high pressure center.

### 5.1.3 Nocturnal Wind Profile

To obtain the height-time cross sections, the wind speeds/directions were plotted and analyzed by hand. In each of the nocturnal wind profiles to follow the analysis will begin at 1800 CST on the evening prior to the helicopter spiral and will end at 0800 CST on the morning of the helicopter spiral. The analysis for day 215 actually begins at 1800 CST on day 214 and continues until 0800 CST on day 215. The analysis for day 215 is shown in Figure 5.3a and b. The shaded regions in the figure indicate levels at which the temperature was increasing with height (an inversion) as determined by radiosonde measurements (site 144) at 2200 and 0400 CST and by helicopter measurements over Smartt Field at the other times indicated.

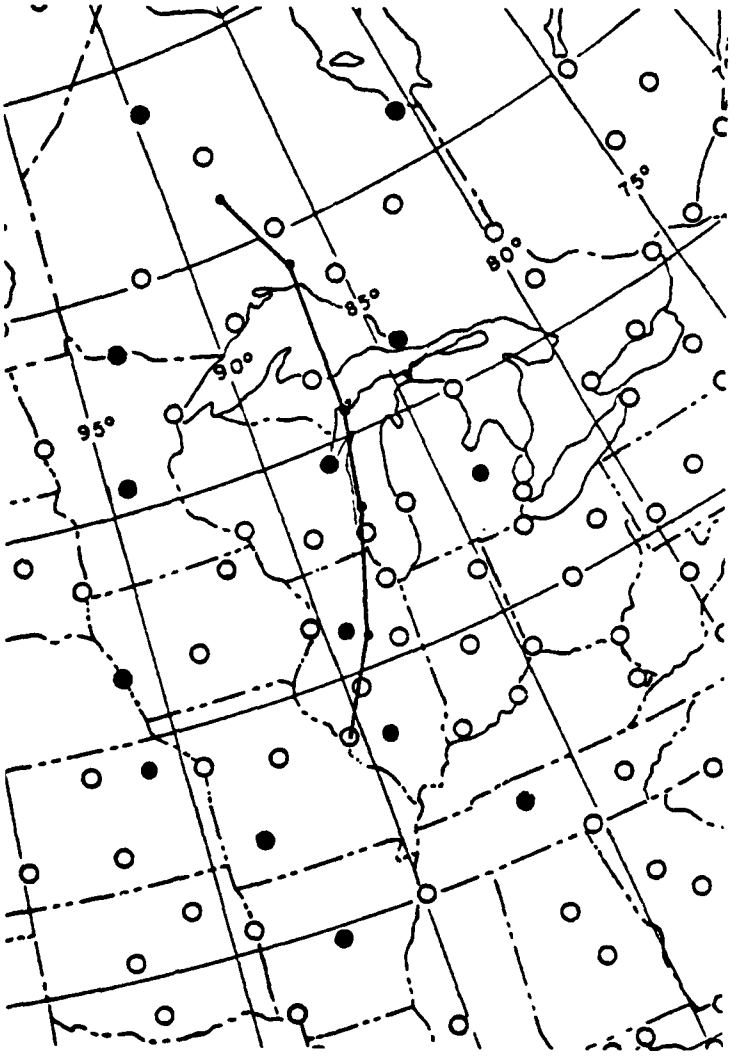


Figure 5.2 Layer-average trajectory for day 215. Maximum top of layer is 2000 m. Base of the layer is chosen by the trajectory model. "•" indicates a radiosonde station within 300 nm (approximately 550 km) of trajectory. Each segment represents 12 hours.

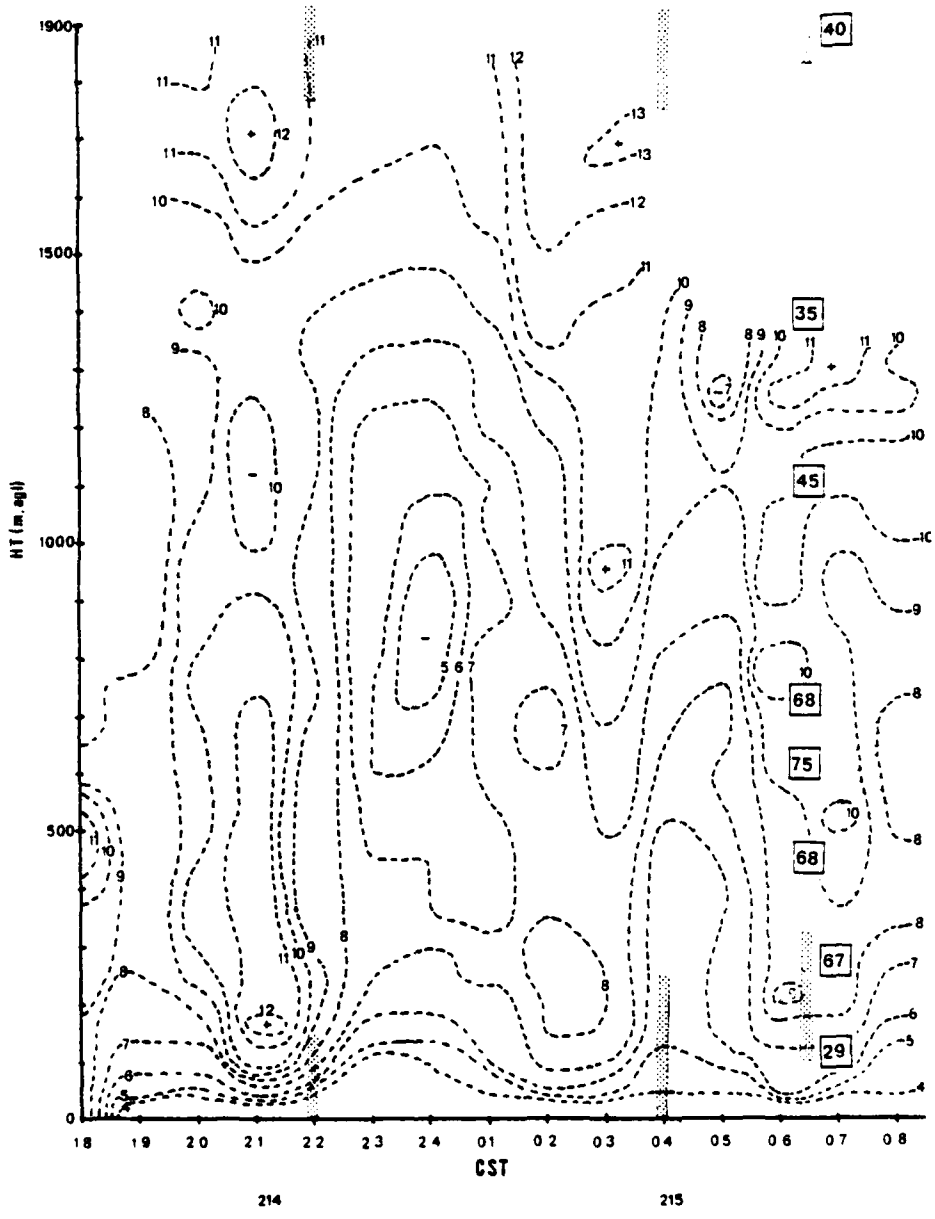


Figure 5.3a Height-time section of wind speed ($m\ s^{-1}$) for day 215. Shaded area represents an inversion. A "+" indicates a wind speed maximum. A "-" indicates a wind speed minimum. □ indicates ozone concentration in ppb.

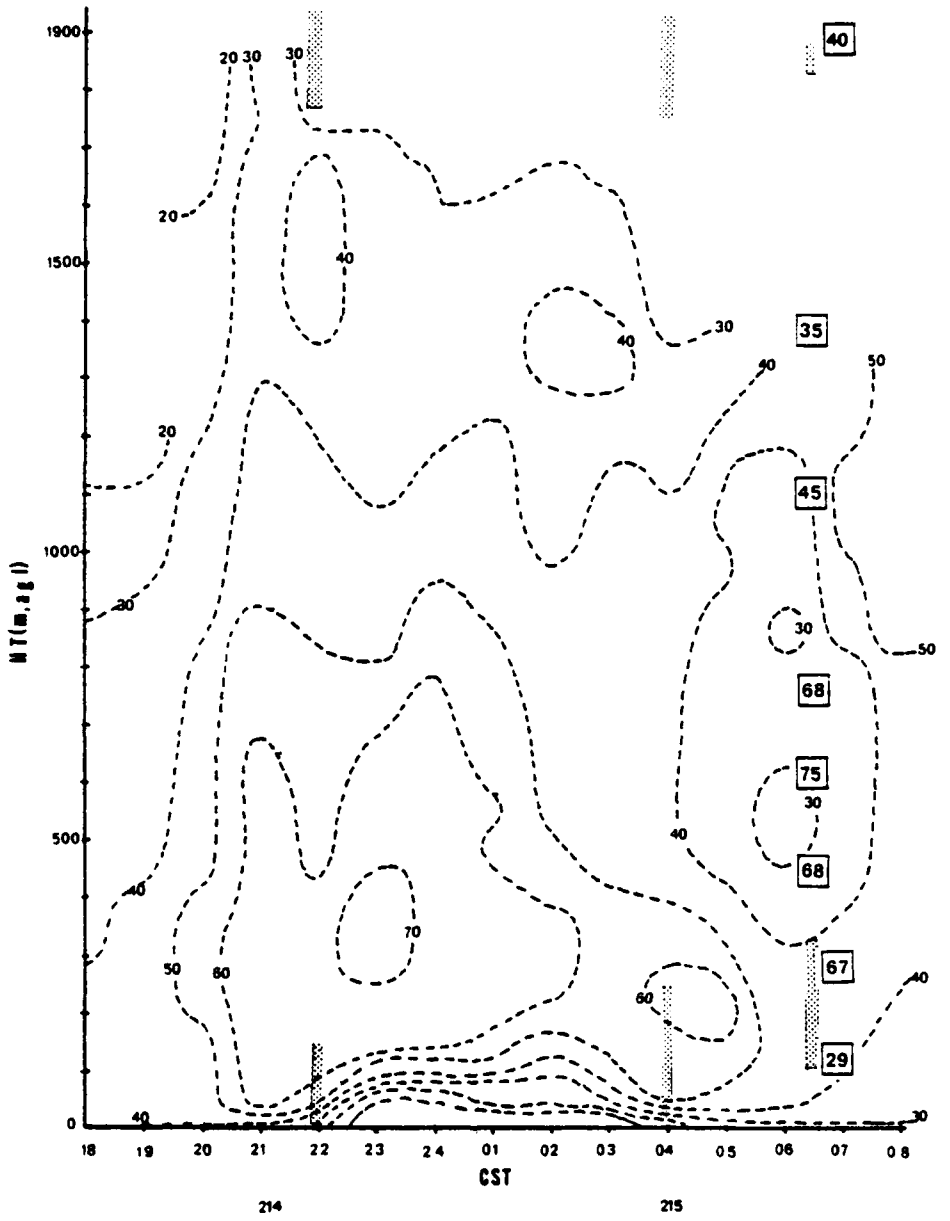


Figure 5.3b Height-time section of wind direction for day 215. Shaded area represents an inversion. Wind direction in degrees. □ indicates ozone concentration in ppb.

Figure 5.3a shows the formation of a low level jet near the top of the nocturnal radiation inversion. The jet remains at 10 to 12 meters per second ($m\,s^{-1}$) throughout the lowest 1800 meters (m). After 2200 CST the winds decrease at all levels, with a speed minimum established between 700 and 1000 m AGL by 2400 CST. By 0300 CST a second wind speed maximum is established at approximately 1700 m AGL and may persist until 0800 CST as evidenced by the maximum at 1300 m and below after 0500 CST.

The wind direction time section for day 215 (Fig. 5.3b) shows the veering of the winds from the surface to the top of the radiation inversion. The wind direction below 1000 m AGL gradually veered during the formation of the nocturnal jet then backed from 070 to 040 degrees between 2400 CST and 0800 CST. The winds above 1500 m AGL, where the upper wind maximum occurred, veered from 020 to 040 degrees between 1800 CST and 0600 CST.

Changes in the nocturnal wind profile will affect the trajectory of an air parcel during the night. However, the trajectory computed in this case and in the cases to follow are based on observed winds obtained from radiosonde observations. The stations which make up the National Weather Service Radiosonde Network are approximately 450 km apart, on the average, and the soundings are taken twice daily, at 0000 and 1200 GMT (1800 and 0600 CST, respectively). A few stations in the network take PIBAL soundings at 0600 and 1800 GMT (0000 and 1200 CST, respectively), but these are widely scattered and would not contribute significantly to most trajectory calculations.

Figure 5.3a shows that a significant wind speed maximum extending from the top of the radiation inversion to the base of the subsidence inversion has formed by 2100 CST. By 2400 CST the jet has dissipated and prior to 0600 CST reforms near the base of the subsidence inversion. Figure 5.3b shows the gradual veering of the winds after 1800 CST, especially in the layer from the top of the radiation inversion to approximately 800 m AGL. These changes, occurring between 1800 and 0600 CST, would not have been detected by radiosonde measurements taken by the National Weather Service network of stations. Therefore, the trajectories computed by the Heffter-Taylor Model will not reflect the changes which occur between radiosonde launches.

In order to account for the vertical variability in the nocturnal wind field, trajectories were computed by the Heffter-Taylor Trajectory Model for three 200 m layers. The first layer was from 200 to 400 m AGL, the second from 900 to 1100 m AGL, and the third from 1700 to 1900 m AGL (Figure 5.4). The first 12-hour segment for the 200 to 400 m layer was compared to a hand computed trajectory which was obtained from the hourly PIBAL soundings taken at site 144 ( "★" in Figure 5.4).

Figure 5.4 shows that the hand computed trajectory and the computer trajectory do not follow the same path. Figure 5.3b shows that the winds in the layer 200-400 m AGL veer from 1800 CST to approximately 0500 CST with some backing between 0500 and 0800 CST. The directional shear in the 200-400 m AGL layer after 1800 CST and before 0600 CST would account for the differences in the hand computed and computer produced trajectories.

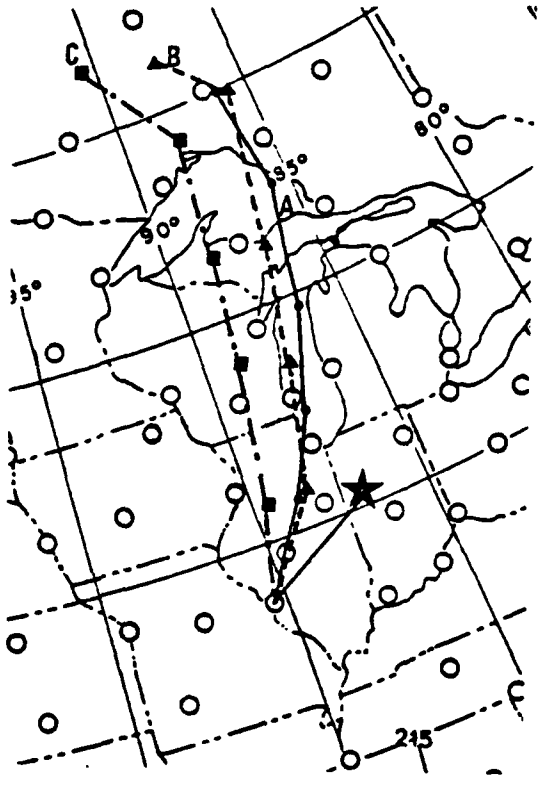


Figure 5.4 200 m-layer average trajectory for day 215. Trajectory A is for 200-400 m AGL layer, Trajectory B is for 900-1100 m AGL layer, and Trajectory C is for 1700-1900 m AGL layer. "★" indicates the end point of the 12-hour hand computed 200-400 m AGL trajectory. Each segment represents 12 hours.

In this case and the cases to follow the comparison between the trajectories (primarily the segments 24 hours prior to arrival over St. Louis) will be described in terms of how much the size of the possible source region changes when the three 200 m-layer trajectories are compared to the original layer-average trajectory (maximum layer top at 2000 m) with the hand computed trajectory used as an indication of the nocturnal variability of the wind field.

Comparison of Figures 5.2 and 5.4 indicates that the 200-400 m and 900-1100 m AGL layer trajectories and the original layer average trajectory (maximum layer top 2000 m AGL) follow almost the same path on day 215. The 12-hour hand computed trajectory indicates that at least the 200-400 m AGL layer trajectory should be moved eastward. However, the accuracy of hand computed trajectories based on winds at a single point is highly suspect beyond 12 hours. The 1700-1900 m AGL trajectory takes a more northerly course remaining to the west of the other trajectories. Therefore, even if the hand computed trajectory is not considered, the source region has been redefined to lie in a region outlined by the three 200 m-layer trajectories as compared to the single path given by the original layer average trajectory.

Comparison of the 12-hour positions of the 200-400 m AGL trajectory as determined by hand and by computer model will be presented in each of the cases to follow. Even though hourly PIBAL and radiosonde observations from existing upper-air stations would better describe the wind field, they would not insure that computer models were able to produce trajectories that were entirely representative. The reason for this is that the coarse spatial resolution and variability of network stations

is as important as the lack of temporal resolution of the observations. The irregular spacing of stations and the omission of data from some reporting stations could allow significant small scale phenomena to occur without detection.

In addition, a meaningful choice of layers would be very difficult because of vertical motion which might be present. As an example, the pollutant which was observed in the 200-400 m AGL layer over Smartt Field may very well have been in a layer between 1200 and 1400 m AGL 24-hours earlier upwind of Smartt Field. Thus, the 200-400 m AGL layer trajectory may indicate the wrong source region for the pollutant in that layer over Smartt Field.

Therefore, care must be taken not to state that the trajectory indicates that the pollutant burden of an air sample is due to a specific site, such as Chicago, Illinois. However, the trajectory analysis could be used to indicate a source region such as the area around southern Lake Michigan which might be defined to stretch from Milwaukee on the west bank of Lake Michigan, south to the Chicago-Gary area, then north along the east coast of Lake Michigan to the same latitude as Milwaukee. In some cases even this area would be too small, depending on the vertical variability of the wind field.

### 5.1.4 Ozone Profile

Figure 5.5 shows the vertical profile of $O_3$, NO, $NO_x$, and temperature. The mixing height upwind of St. Louis on the previous afternoon is denoted by "MH" on the left vertical axis. The upwind location was determined by the Heffter-Taylor Trajectory Model for a layer whose maximum top is held constant at 2000 m AGL. The radiosonde observation

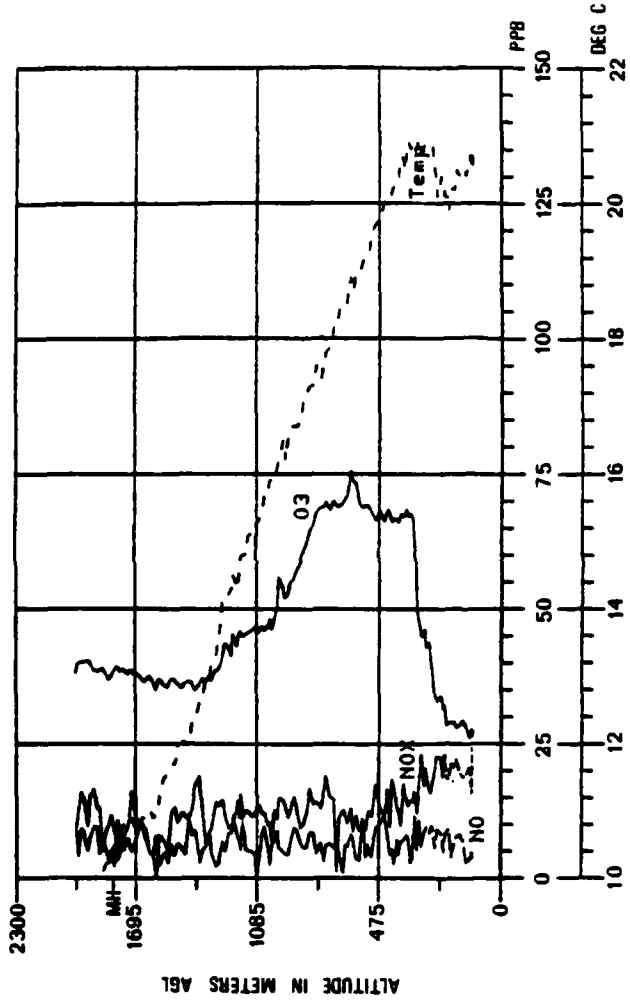


Figure 5.5 Ozone, NO, $NO_x$, and temperature versus altitude, day 215. Upward spiral over Smartt Field between 0625 and 0636 CST. "MH" indicates mixing height on the previous afternoon upwind of Smartt Field.

nearest to the end of the first 12-hour segment upwind of St. Louis was used to compute the afternoon's mixing height. In four of the five cases Peoria, Illinois, was used as the representative radiosonde station, the exception was on day 217 for which St. Louis was chosen as the most representative station.

On day 215 (Figure 5.5) a decrease in the ozone concentration occurs well below the mixing height established the previous afternoon. According to Ludwig (1979a), the ozone should have been uniformly mixed up to the mixing height on the previous day in the region where the pollutant was emitted.

The decrease in the ozone below the low-level radiation inversion is probably due to a combination of dry deposition and $NO_x$ scavenging as evidenced by the increased levels of $NO_x$ below the top of the inversion. The vertical concentration of ozone above the radiation inversion remains nearly constant with height up to approximately 800 m AGL. Above 800 m AGL the ozone concentration decreases until it reaches background levels at approximately 1400 m AGL.

A representative sample of the vertical concentration of ozone is plotted at the time of the helicopter flight (0625 CST) in Figure 5.3a and b. The profile indicates that little or no directional shear exists at the levels where the ozone concentration decreases. The wind speeds are also uniform in the levels where the ozone concentration is uniform as well as in the layers where the ozone concentration decreases.

## 5.2 Case II: Day 216

### 5.2.1 Synoptic Chart Discussion

By 0600 CST on day 216 (Figure 5.6) the high pressure center, located over North Dakota on day 215, had moved southwestward to the southern tip of Lake Michigan, with a second center over northern Pennsylvania and southern New York. A flat pressure field extended from the east coast to the Rocky Mountains and from the northern Great Lakes to southern Tennessee and Arkansas.

By 0600 CST on day 216 the 850 mb high was over eastern Iowa with a flat pressure field covering Iowa, Missouri, Illinois, Indiana, Ohio and parts of surrounding states.

By 0600 CST on day 216 the 700 mb flow over Missouri was dominated by a 700 mb high over Texas and a weak trough over the eastern one-third of the United States.

By day 216 the flow into St. Louis remained northerly but weakened due to the flat pressure gradient that became established at the surface and 850 mb. The 700 mb flow remained from the north-northwest.

### 5.2.2 Trajectory Analysis

The layer-average wind trajectory for day 216 is shown in Figure 5.7. The trajectory begins to the north of Lake Superior, moves southeastward to eastern Wisconsin, then moves along a south-southwestward path to St. Louis. The total distance covered by the trajectory was approximately 1300 km.

The trajectory segments for day 216 are nearly uniform for the first 36 hours (60 to 24 hours prior to arriving over St. Louis), but

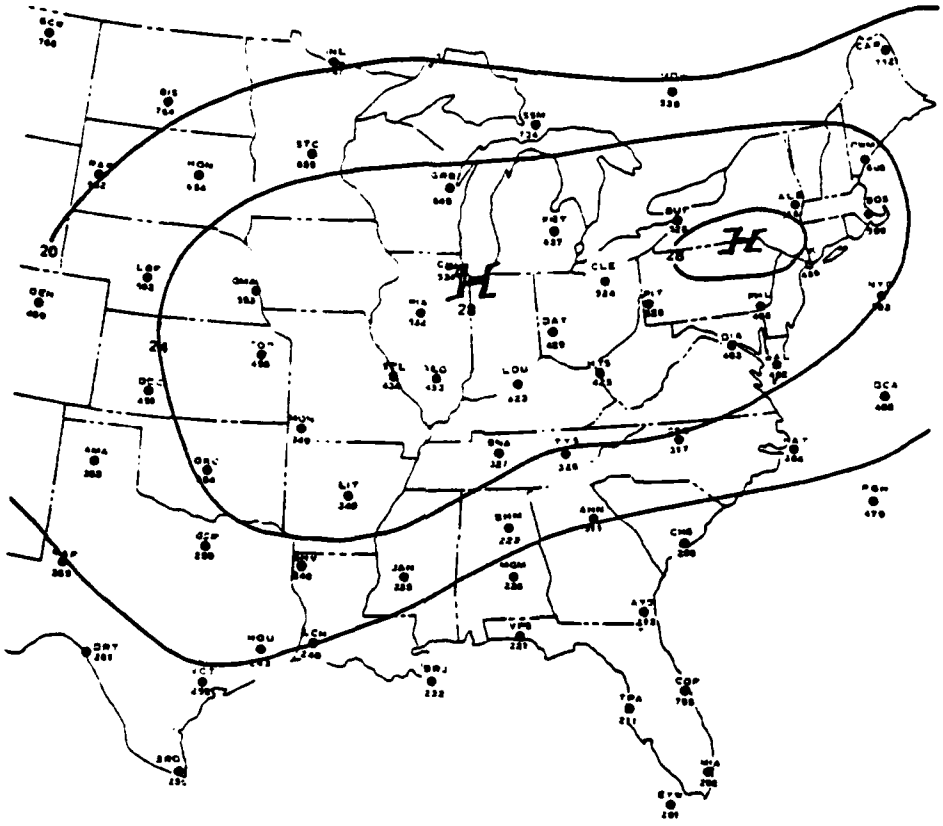

Figure 5.6 Surface analysis for day 216 at 0600 CST

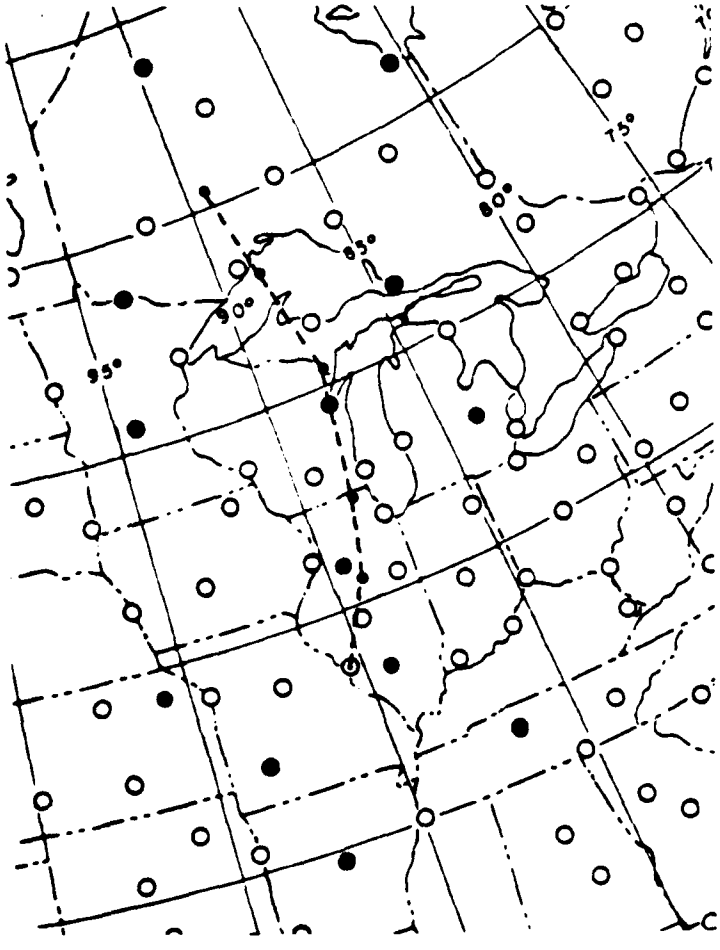


Figure 5.7 Layer-average trajectory for day 216. Maximum top of layer is 2000 m; base of the layer is chosen by the trajectory model. "•" indicates a radiosonde station within 300 nm (approximately 550 km) of trajectory. Each segment represents 12 hours.

become shorter during the last 24 hours as the high pressure center becomes established near Chicago.

5.2.3 Nocturnal Wind Profile

The height-time sections of wind speed and direction were obtained as described in Case I. The height-time sections for day 216 are shown in Figures 5.8a and b.

Figure 5.8a shows the formation of the wind speed maxima (jet) above the top of the radiation inversion. Unlike day 215, the well-defined jet persists at speeds greater than or equal to 11 $m\,s^{-1}$ from 2000 to 0200 CST and dominates the lower 1 km. The jet decreases in speed and rises as the inversion rises between 0200 and 0400 CST. A small jet appears at approximately 200 m AGL between 0500 and 0700 CST. A wind speed maximum appears between 1700 and 1800 m AGL between 0100 and 0300 CST and lowers as the base of the subsidence inversion lowers during the early morning.

Figure 5.8b shows a layer of pronounced directional shear extending down from about 1600 m AGL at 1900 CST to about 500 m AGL at 0600 CST. This layer of maximum directional shear occurs in a layer of speed minimum in Figure 5.8a. In addition, the lowering of the shear zone to its lowest point and the decrease of wind speeds in the nocturnal jet to a minimum value occur almost simultaneously. The winds below the shear layer underwent a gradual veering between 1900 and 0600 CST, with the greatest amount of veering occurring at the height of the maximum wind speeds.

Figures 5.8a and b show that the significant changes which occur in the nocturnal wind field take place after the 1800 CST radiosonde

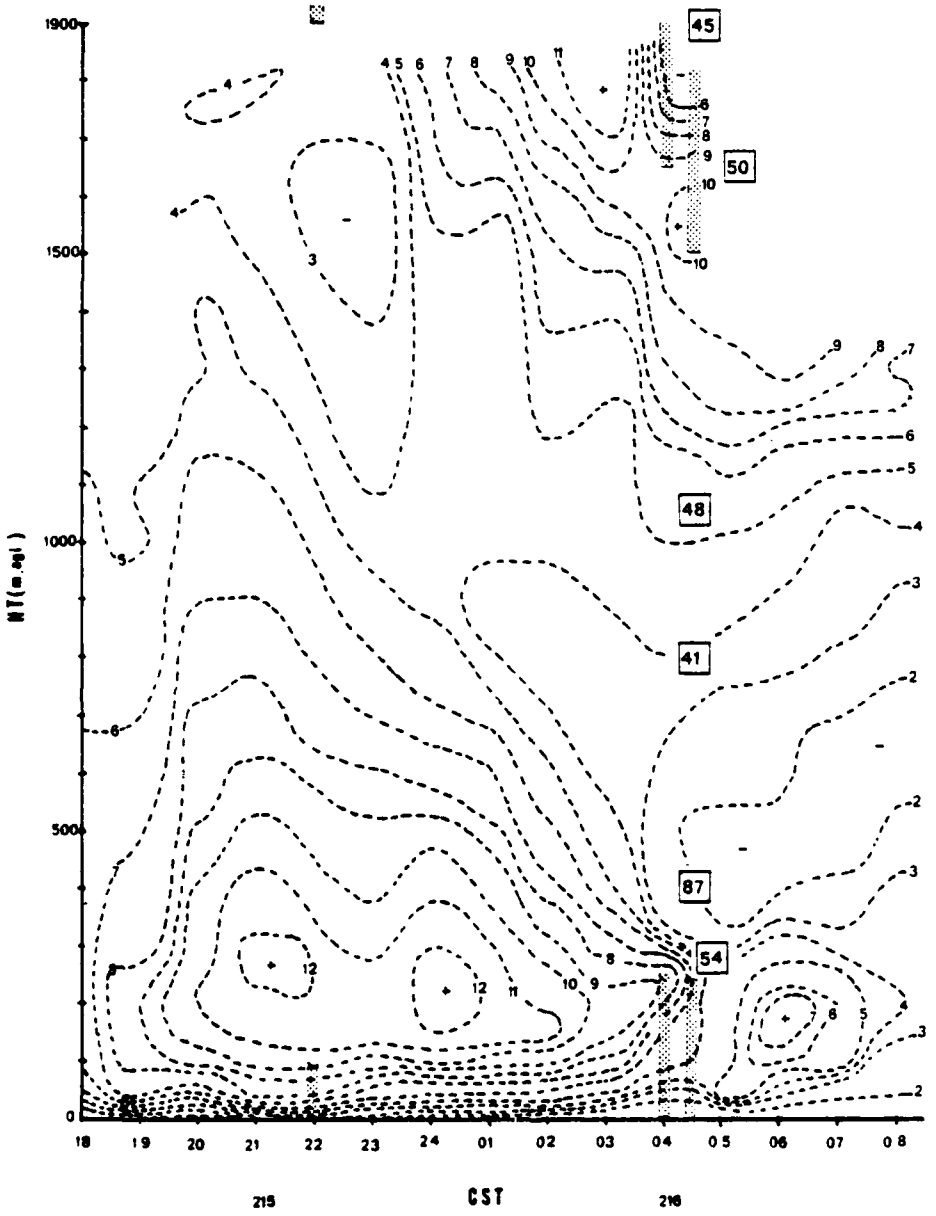


Figure 5.8a Height-time section of wind speed (m $s^{-1}$) for day 216. Shaded area represents an inversion. A "+" indicates a wind speed maximum. A "-" indicates a wind speed minimum. □ indicates ozone concentration in ppb.

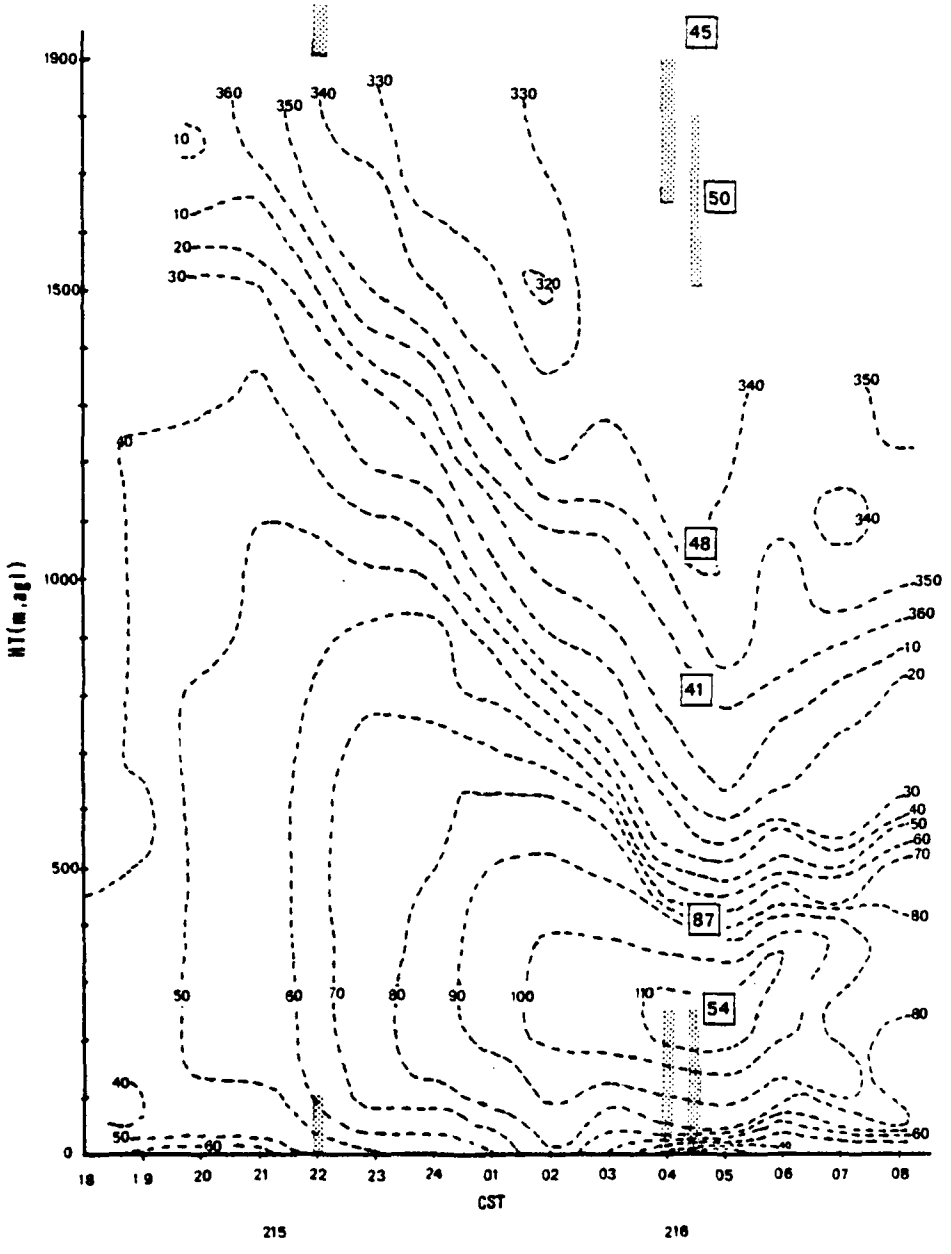


Figure 5.8b Height-time section of wind direction for day 216. Shaded area represents an inversion. Wind direction in degrees. □ indicates ozone concentration in ppb.

launch. The changes in the wind direction are still evident at the scheduled 0600 CST radiosonde launch but the wind speed in the nocturnal jet has decreased to 6 $m s^{-1}$ as opposed to the 12 $m s^{-1}$ observed during the night.

Figure 5.9 shows the three 200 m-layer trajectories and the 12-hour hand computed trajectory for day 216. In the layer from 200 to 400 m AGL the differences between the hand computed and the computer produced trajectory is very large. Figure 5.8b shows that in the layer from 200-400 m AGL the winds veered between 1800 CST and approximately 0600 CST, with backing occurring after 0600 CST. The fact that the trajectory model did not account for the continued veering may have been caused by the requirement that all radiosonde observations within a 300 nautical mile (550 km) radius be averaged to compute a trajectory segment. This would tend to mask a small scale feature such as a nocturnal jet and any associated directional shear. The difference in the 900-1100 m AGL and 1700-1900 m AGL layers would not be as great as in the 200-400 m AGL layer.

A comparison of Figures 5.7 and 5.9 indicates that the original trajectory (maximum layer top 2000 m AGL) follows a path which is between the 900-1100 m and the 1700-1900 m AGL trajectories. The 12-hour hand computed trajectory indicates that the 200-400 m AGL layer trajectory should be moved eastward. Even if the hand computed trajectory is not considered, the source region has been redefined and is outlined by the three 200 m-layer trajectories. However, due to the large difference between the hand computed and computer produced 200-400 m AGL layer trajectory the eastern boundary of the source region is uncertain.

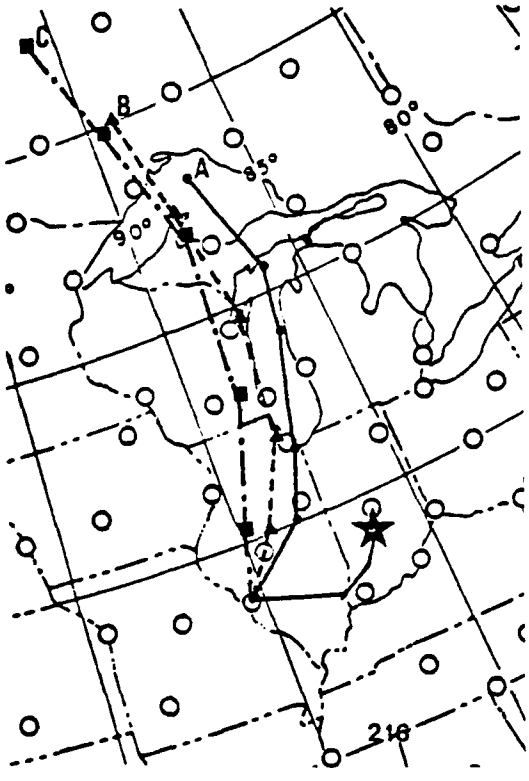


Figure 5.9 200 m-layer average trajectory for day 216. Trajectory A is for 200-400 m AGL layer, Trajectory B is for 900-1100 m AGL layer, and Trajectory C is for 1700-1900 m AGL layer. "★" indicates the end point of the 12-hour computed 200-400 m AGL trajectory. Each segment represents 12 hours.

5.2.4 Ozone Profile

Figure 5.10 shows the vertical profile of $O_3$, NO, $NO_x$, and temperature for day 216.

On day 216 the decrease in the ozone concentration occurs well below the mixing height established the previous afternoon. As described in Case I, the ozone was expected to be uniformly mixed up to the mixing height on the previous day in the region where the pollutant was emitted.

The vertical profile of ozone concentration for the 0435 CST spiral on day 216 (Figure 5.10) shows a sharp spike of ozone just above the top of the radiation inversion. The sharp decrease of ozone between the inversion and the maximum measured concentration is probably due to $NO_x$ scavenging from a power plant plume. The ensuing downward helicopter spiral over Smartt Field beginning at 0448 CST (Figure 4.1a) indicates two distinct $NO_x$ plumes, one below the top of the radiation inversion and the other between the top of the radiation inversion and the maximum ozone concentration. The decrease in the ozone concentration above the measured maximum does not exhibit the very rapid decrease in ozone as would be associated with a $NO_x$ plume.

Figure 5.8b also contains a representative sample of the vertical concentration of ozone plotted at the time of the helicopter flight (0435 CST). Notice that the measured ozone maximum (87 ppb) occurs near the bottom of the shear layer and that between the maximum concentration and the next minimum (41 ppb) there is approximately 90 degrees of directional shear. Above the minimum, which is located at approximately 800 m AGL, there is relatively little directional shear and little change in ozone concentrations.

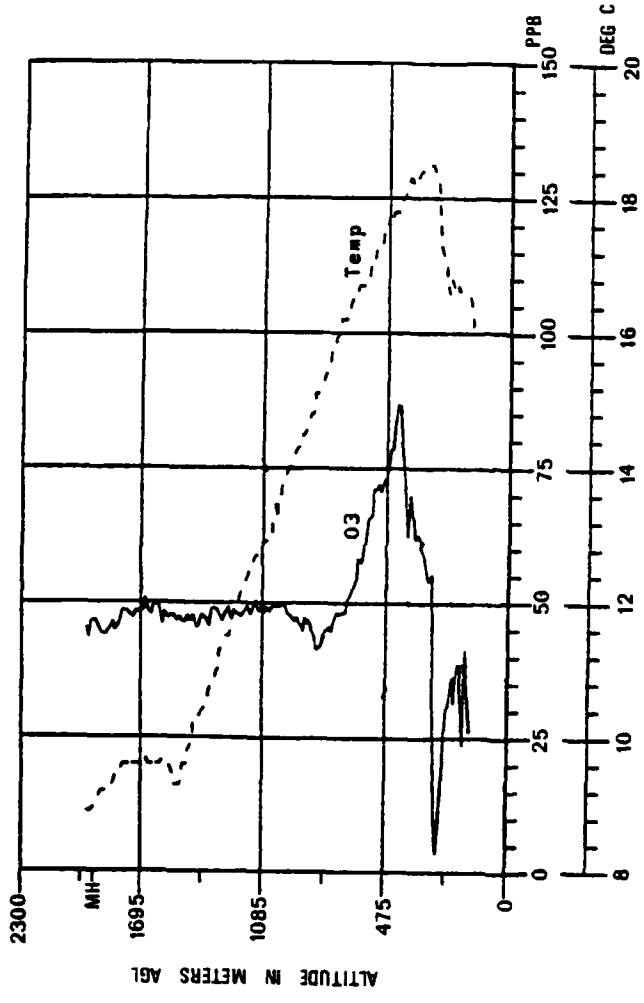


Figure 5.10 Ozone and temperature versus altitude, day 216. Upward spiral over Smartt Field between 0435 and 0448 CST. "MH" indicates mixing height on the previous afternoon upwind of Smartt Field. NO and $NO_x$ data not available.

Figure 5.8a also contains a representative sample of the vertical concentration of ozone plotted at the time of the helicopter flight. The ozone maximum (87 ppb) occurs in a wind speed minimum at approximately the same height as the wind speed maximum which occurred previously that night.

## 5.3 Case III: Day 217

### 5.3.1 Synoptic Chart Discussion

By 0600 CST on day 217 (Figure 5.11) the high pressure center at the southern tip of Lake Michigan on day 216 had moved southwest to be located just to the east of St. Louis and had weakened. The high pressure center in the east drifted to eastern Pennsylvania and also weakened. A flat pressure gradient extended from the east coast across Illinois and then southwestward to Texas.

The flat height field at 850 mb covered an area extending from Texas in the Southwest across central and southern Missouri to New Hampshire in the Northeast as well as the Mid-Atlantic and Southeastern States by 0600 CST on day 217.

The gradient of the 700 mb height field increases as far south as northern Missouri by 0600 CST on day 217 with a relatively flat height field remaining over Missouri and southward to the Gulf of Mexico. Lack of appreciable gradients over eastern Missouri at all heights up to 700 mb would be associated with light winds through a deep layer over that region.

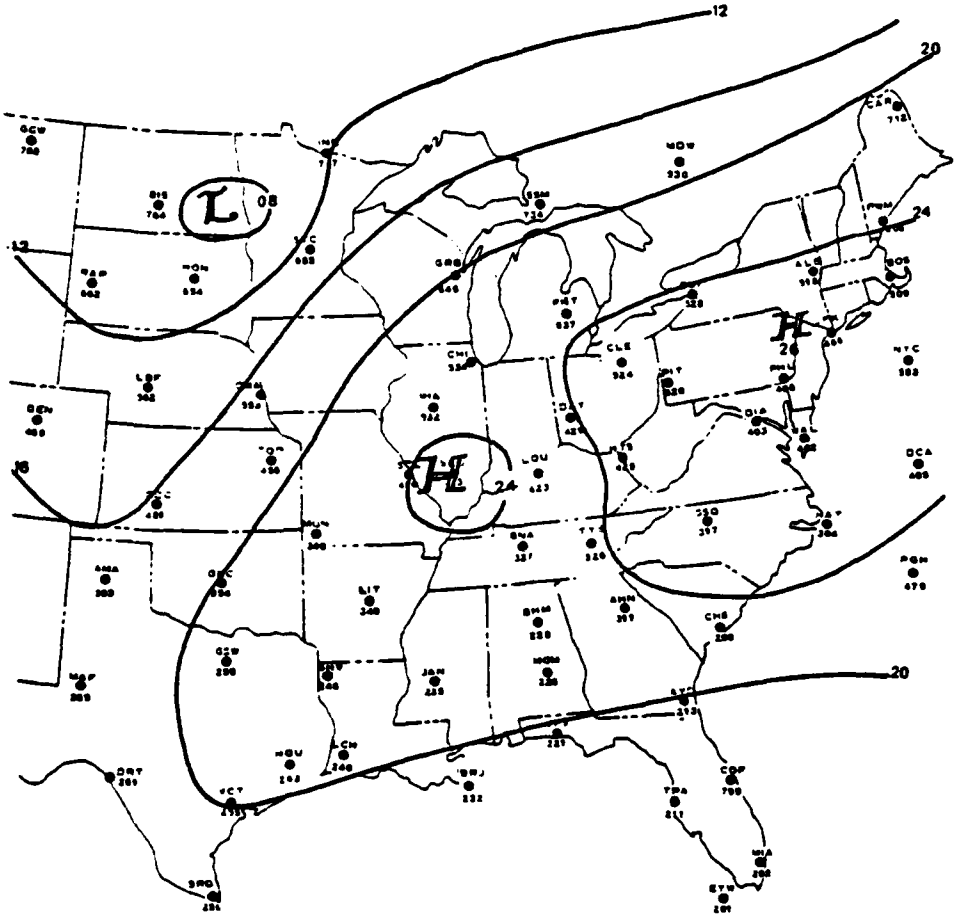


Figure 5.11 Surface analysis for day 217 at 0600 CST

### 5.3.2 Trajectory Analysis

The layer-average wind trajectory for day 217 is shown in Figure 5.12. The trajectory begins near the southern most point of the upper peninsula of Michigan, moves south-southwestward passing near St. Louis at 0600 CST on day 216 before arriving over St. Louis, from the south, on the morning of day 217. According to Hoecker (1977), the bias correction for southerly flow is approximately an 8 degree direction backing adjustment. The error distance associated with the short southerly trajectory segment for day 217 would be approximately 10 km if the bias correction were applied.

The trajectory segments for day 217 become progressively shorter after the first 12 hours (48 hours prior to St. Louis) as the high center becomes established over Illinois and drifts south to be east of St. Louis by 0600 CST on day 217. The total distance covered by the trajectory for day 217 is 1100 km which is shorter than the distance covered by the trajectories for days 215 and 216.

### 5.3.3 Nocturnal Wind Profile

The height-time sections of wind speed and direction were obtained as described in Case I. The height-time sections for day 217 are shown in Figures 5.13a and b.

Figure 5.13a shows that after 2000 CST a nocturnal jet with a max speed of 8 $m\,s^{-1}$ becomes established at the top of the radiation inversion and changes little throughout the night. A secondary speed maximum occurs near the base of the subsidence inversion and persists until at least 0300 CST, afterwhich the data above 1300 m AGL are no longer available.

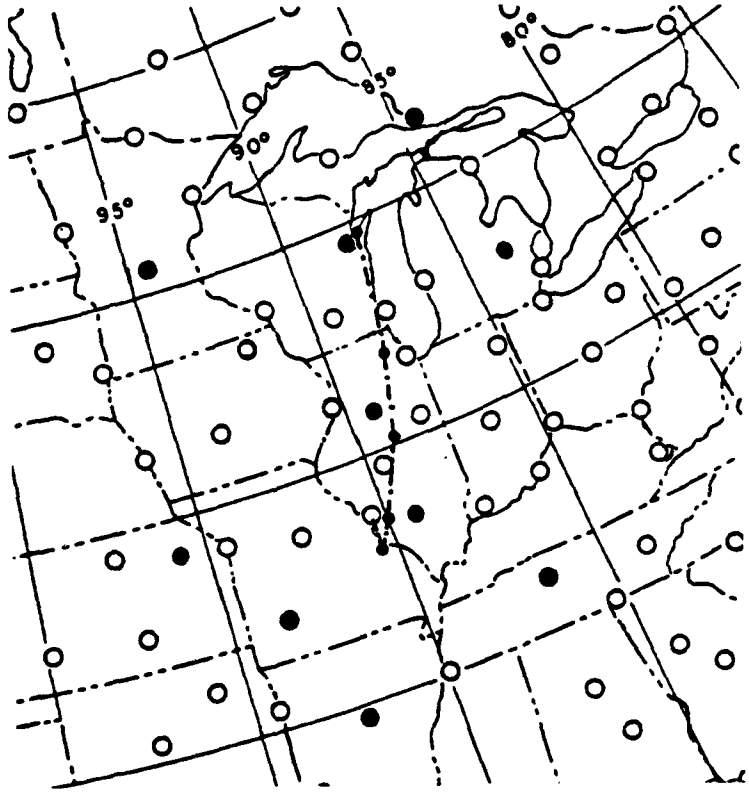


Figure 5.12 Layer-average trajectory for day 217. Maximum top of layer is 2000 m; base of the layer is chosen by the trajectory model. "•" indicates a radiosonde station within 300 nm (approximately 550 km) of trajectory. Each segment represents 12 hours.

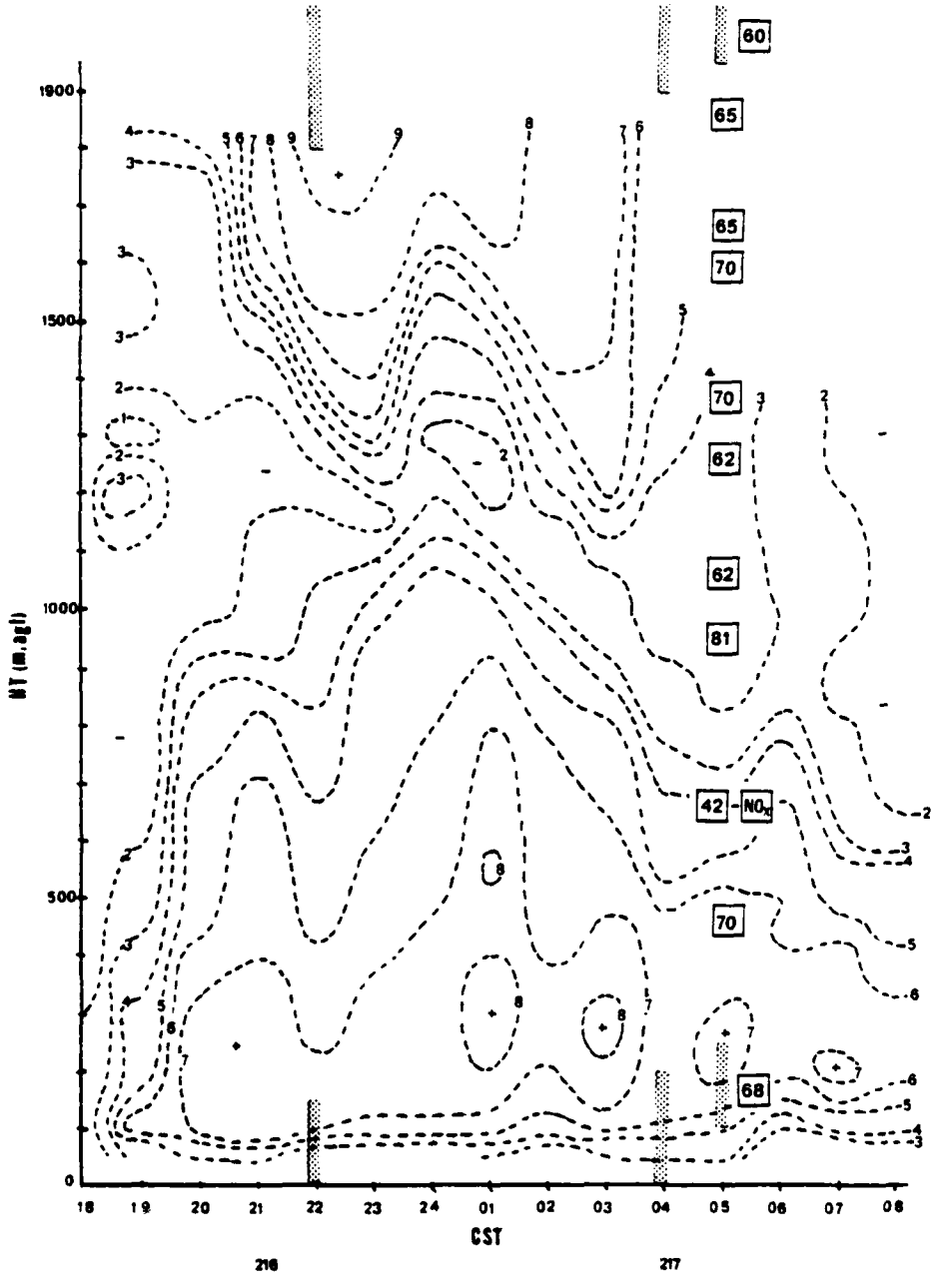


Figure 5.13a Height-time section of wind speed ($m\ s^{-1}$) for day 217. Shaded area represents an inversion. A "+" indicates a wind speed maximum. A "-" indicates a wind speed minimum. ☐ indicates ozone concentration in ppb.

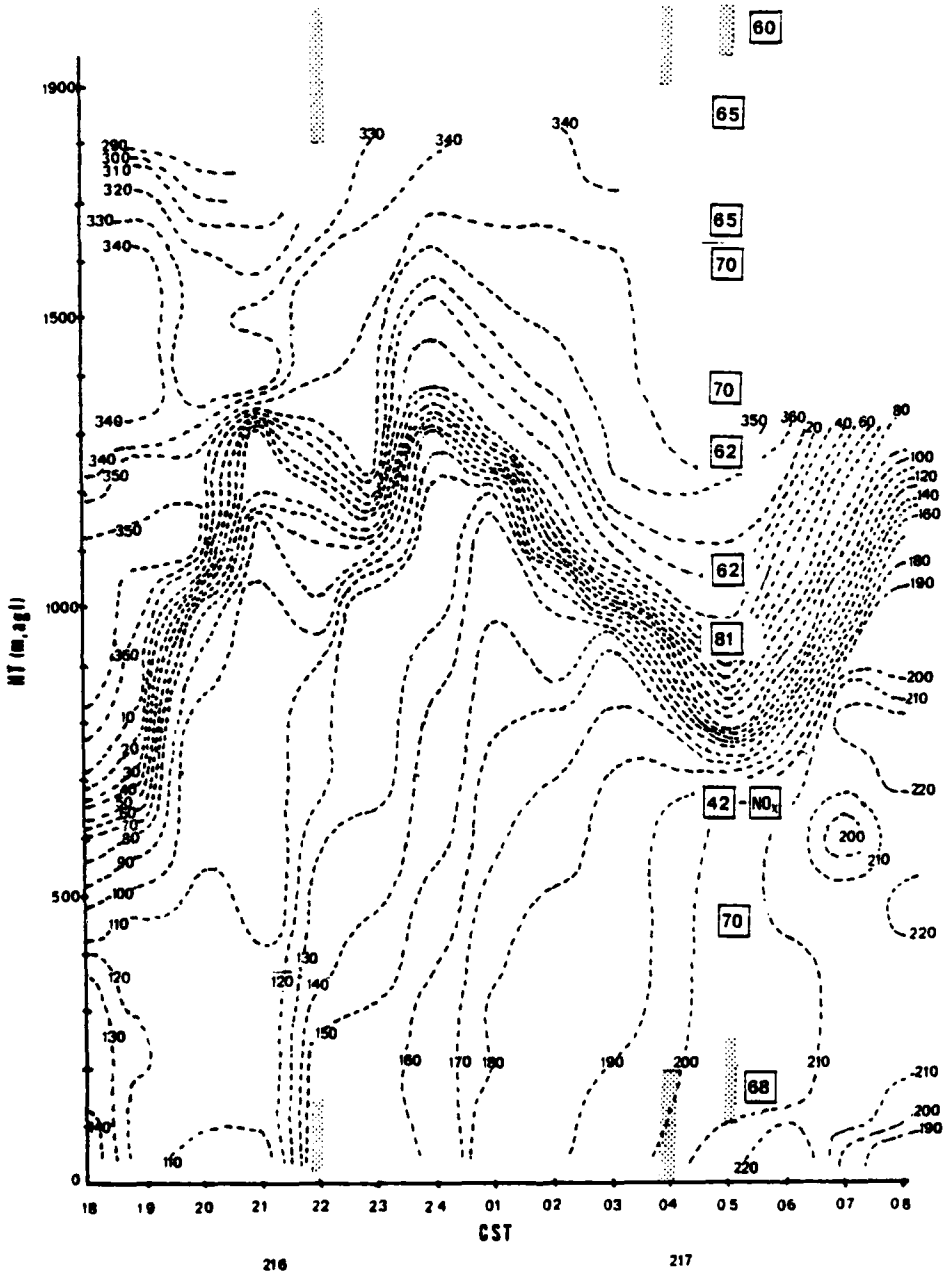


Figure 5.13b Height-time section of wind direction for day 217. Shaded area represents an inversion. Wind direction in degrees. □indicates ozone concentration in ppb.

The wind direction height-time section for day 217 (Figure 5.13b) depicts a very pronounced layer of persistent directional shear which rises between 1900 and 2400 CST, then sinks to its lowest level at 0500 CST before rising again. Below the layer of directional shear there is a gradual veering of the winds throughout the night. Above the layer of directional shear comparatively little change occurs in the wind direction.

Figures 5.13a and b show that the wind field is highly variable between scheduled radiosonde launch times (1800 and 0600 CST). The wind speed cross section indicates that a nocturnal jet with a maximum speed of 8 m $s^{-1}$ forms after 1800 CST but is still present as a 7 m $s^{-1}$ jet at 0600 CST. The directional shear is the most pronounced and the most variable change which takes place between 1800 and 0600 CST.

Figure 5.14 shows the three 200 m-layer trajectories and the 12-hour hand computed trajectory for the 200-400 m AGL layer for day 217. The hand computed and computer produced trajectories for the 200-400 m AGL layer are along almost the same path. This agreement is due to the very gradual but slight veering that occurred between 1800 and 0600 CST (Figure 5.13b). The hand computed trajectory indicates that the air parcel traveled a much greater distance (approximately 185 km) than is indicated by the computer produced trajectory. This is due, at least in part, to the formation of the 8 m $s^{-1}$ nocturnal jet between 2400 CST and 0400 CST. The 0600 CST radiosonde would have detected 6 to 7 m $s^{-1}$ winds, but the 1800 CST radiosonde would have detected only 2 to 3 m $s^{-1}$ winds. The 900-1100 m AGL trajectory is representative since, even though directional shear is present, the winds are extremely light.

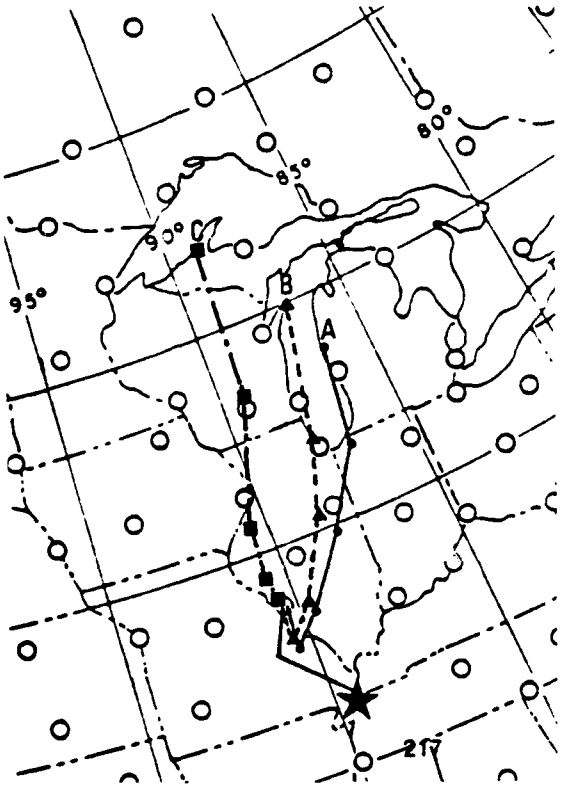


Figure 5.14 200 m-layer average trajectory for day 217. Trajectory A is for 200-400 m AGL layer, Trajectory B is for 900-1100 m AGL layer, and Trajectory C is for 1700-1900 m AGL layer. "★" indicates the end point of the 12-hour hand computed 200-400 m AGL trajectory. Each segment represents 12 hours.

The 1700-1900 m AGL computer produced trajectory does not account for the changes in wind speed which took place during the night. The direction from which the parcel moved appears consistent with more detailed information available at these levels in Figure 5.13b.

Figures 5.12 and 5.14 indicate that the trajectories for the 200-400 m and 900-1100 m AGL layers are in agreement with the original layer average trajectory (maximum layer top 2000 m). The 1700-1900 m AGL layer trajectory indicates almost no movement during the first 12 hours and then a northerly trajectory after that. As already discussed, the first 12-hour segment for the 1700-1900 m AGL layer should have been much longer than predicted by the computer model. The three 200 m-layer trajectories outline a large source region as compared to the single path presented in Figure 5.12. The large deviation of the hand computed trajectory from the 200-400 m AGL computer produced trajectory and the stagnant synoptic situation make the definition of a source region very difficult.

### 5.3.4 Ozone Profile

Figure 5.15 shows the vertical profile of $O_3$, NO, $NO_x$, and temperature for day 217.

The ozone profile for day 217 is similar to the ideal afternoon profile, Type D (Ludwig, 1979a), but does exhibit what appears to be layers of ozone and does not decrease quite as rapidly above the mixing height established the previous afternoon.

The most striking feature in Figure 5.15 is the $NO_x$ plume with a maximum concentration of 42 ppb at 650 m AGL. The maximum ozone concentration of 81 ppb occurs above the $NO_x$ plume at approximately 900

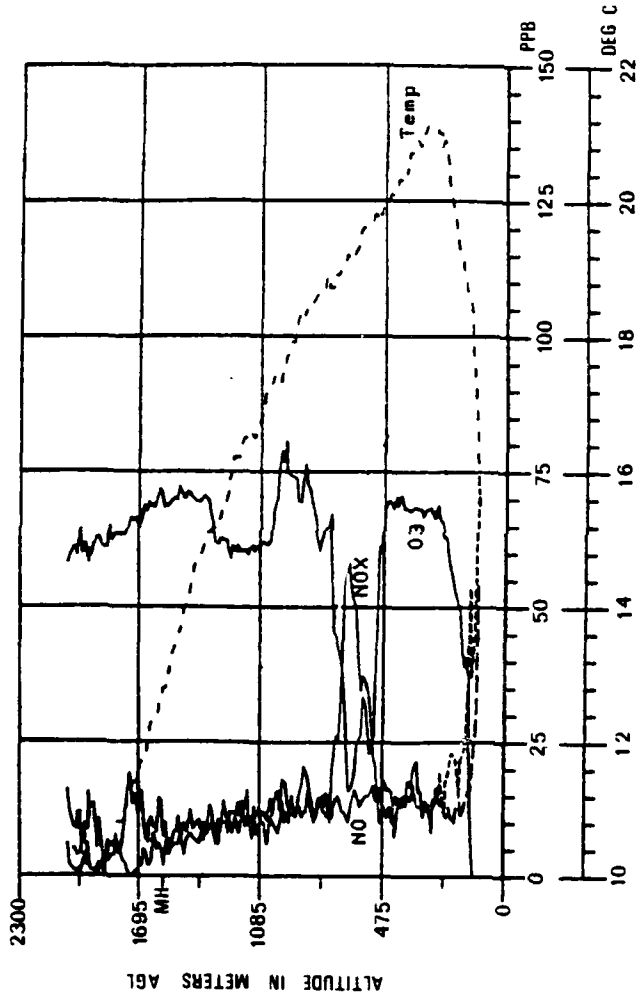


Figure 5.15 Ozone, NO, $NO_x$, and temperature versus altitude, day 217. Upward spiral over Smartt Field between 0504 and 0519 CST. "MH" indicates mixing height on the previous afternoon upwind of Smartt Field.

to 950 m AGL. Above the maximum concentration the ozone decreases rapidly to 62 ppb and remains constant for about 200 meters, then increases to 70 ppb and again decreases to 65 ppb at the base of the subsidence inversion. This is an example of the layers of ozone that exist in the vertical profile on day 217.

Figure 5.13b also contains a representative sample of the vertical concentration of ozone plotted at the time of the helicopter flight (0504 CST). The maximum $NO_x$ concentration (42 ppb) for the helicopter flight is also plotted in the figure. In the layer from the top of the radiation inversion to the level of the $NO_x$ plume the ozone concentration is nearly uniform and the wind direction changes very little. In the layer above the $NO_x$ plume, the wind direction backs from 190 to 030 degrees and the maximum ozone concentration, 81 ppb, decreases to 62 ppb and then increases to 70 ppb. The wind direction between 1300 m and the $NO_x$ plume changes by approximately 210 degrees indicating that decoupling exists between the layers and that several independent layers of ozone could exist.

Figure 5.13a, which also contains a representative sample of the vertical concentration of ozone plotted at the time of the helicopter flight, indicates that the ozone maximum occurs in the region of wind speed minimum, as was observed on day 216.

## 5.4 Case IV: Day 220

### 5.4.1 Synoptic Chart Discussion

The surface analysis for 0600 CST on day 220 (Figure 5.16) indicates a high pressure center near Green Bay, Wisconsin, with an

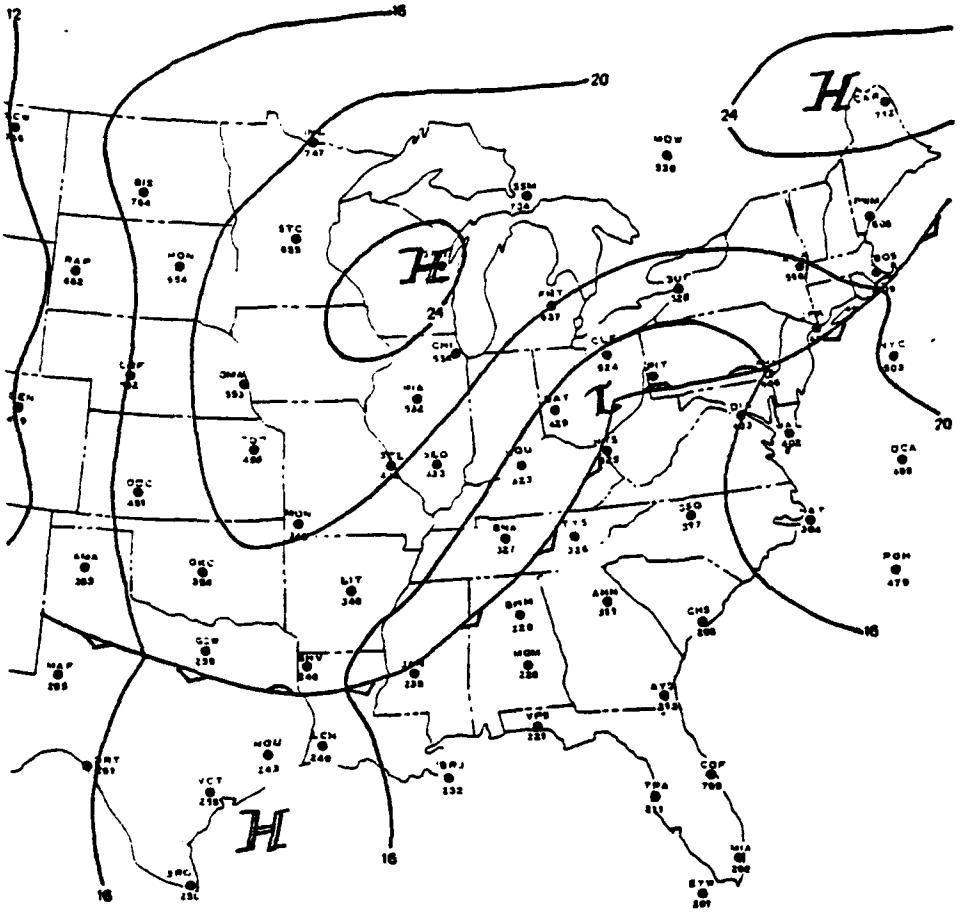


Figure 5.16 Surface analysis for day 220 at 0600 CST

associated ridge extending southwestward across Missouri to Oklahoma. The cold front which passed through St. Louis on day 219 (06 August) extends southwestward from a low pressure center in southeastern Ohio to northern Louisiana. The front becomes stationary and extends across northern Texas to New Mexico.

The 850 mb height analysis for 0600 CST for day 220 indicates a weak ridge of high pressure over western Missouri, with a trough of low pressure extending into eastern Missouri from the northwest.

The 700 mb analysis for 0600 CST on day 220 indicates a high over northern Texas with a ridge extending northward to Minnesota. A low is located in northern Ohio and is dominating the flow pattern from the east coast states to western Missouri.

Thus, the flow from the surface to 850 mb is from the north-northeast over eastern Missouri. At 700 mb a northwesterly flow exists over eastern Missouri.

### 5.4.2 Trajectory Analysis

The layer-average wind trajectory for day 220 is shown in Figure 5.17. The trajectory begins over the western end of Lake Superior and moves east-southeastward to a point where 45 degrees latitude crosses Lake Michigan. The trajectory then moves south-southwestward passing between Milwaukee and Chicago before arriving over St. Louis.

The trajectory exhibits marked anticyclonic curvature during the first 24 hours, with little curvature present during the last 24 hours. The last two trajectory segments are longer than the first three indicating an increase in layer-average winds during the last 24 hours of the trajectory.

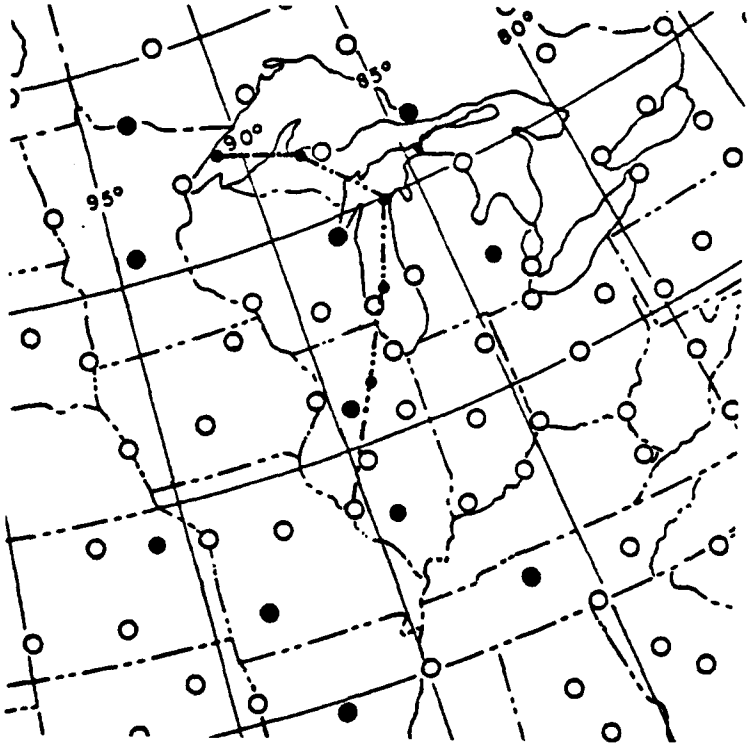


Figure 5.17 Layer-average trajectory for day 220. Maximum top of layer is 2000 m; base of the layer is chosen by the trajectory model. "•" indicates a radiosonde station within 300 nm (approximately 550 km) of trajectory. Each segment represents 12 hours.

5.4.3 Nocturnal Wind Profile

The height-time section of wind speed and direction were obtained as described in Case I. The height-time sections for day 220 are shown in Figures 5.18a and b.

The height-time section for wind speed on day 220 (Figure 5.18a) is complex. A temporary wind speed maximum first forms at approximately 1300 m AGL, then progressively redevelops at lower levels during the night. Between 0400 and 0600 CST the wind speed maximum is located at the top of the radiation inversion (approximately 200 m AGL) with a recorded wind speed of 19 $m\,s^{-1}$. Even though there has been a systematic lowering of the jet during the night, the increase in wind speed to 19 $m\,s^{-1}$ seems questionable. Observers at sites 141, 142, and 143, as shown in Figure 1.1, were also taking hourly PIBAL observations. On day 220 the trajectory into St. Louis was from the north-northeast; therefore, the winds over site 143 are less likely to be affected by the urban heat island than are the winds over site 142. The wind speeds at site 143 were a maximum at approximately 200 m AGL (the same as at site 144) but the maximum speed was approximately 11 $m\,s^{-1}$. The maximum wind speed observed below 500 m AGL at site 144 had ranged from 13 $m\,s^{-1}$ to 11 $m\,s^{-1}$ prior to the 19 $m\,s^{-1}$ observation. In light of this evidence, the wind speed reading of 19 $m\,s^{-1}$ is probably in error and sinds were apparently closer to 11 $m\,s^{-1}$ to 13 $m\,s^{-1}$ at the top of the radiation inversion. By the time of the helicopter flight (approximately 0700 CST) the nocturnal jet had dissipated as the radiation inversion deepened and a second inversion formed between 500 and 600 m AGL.

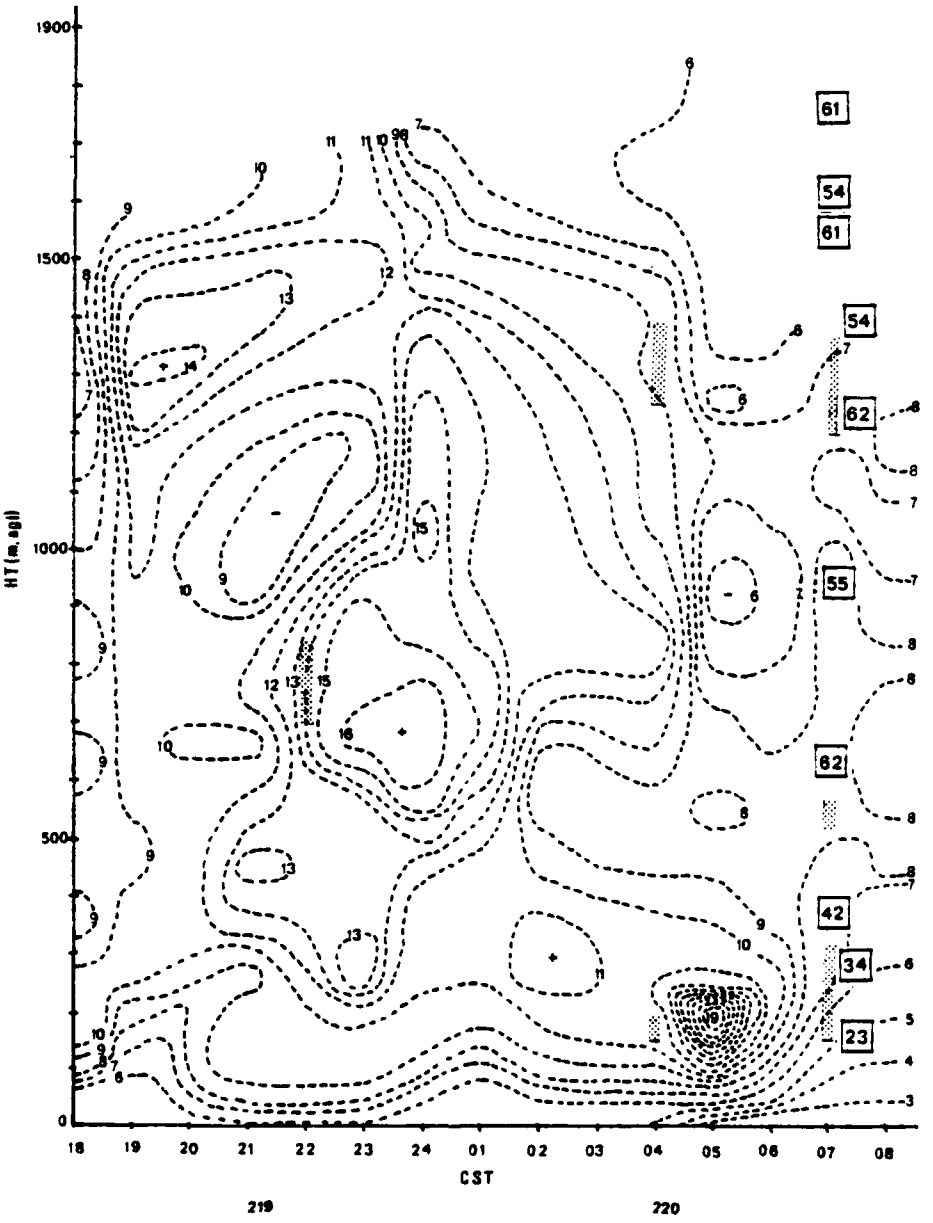


Figure 5.18a Height-time section of wind speed (m $s^{-1}$) for day 220. Shaded area represents an inversion. A "+" indicates a wind speed maximum. A "-" indicates a wind speed minimum. ☐ indicates ozone concentration in ppb.

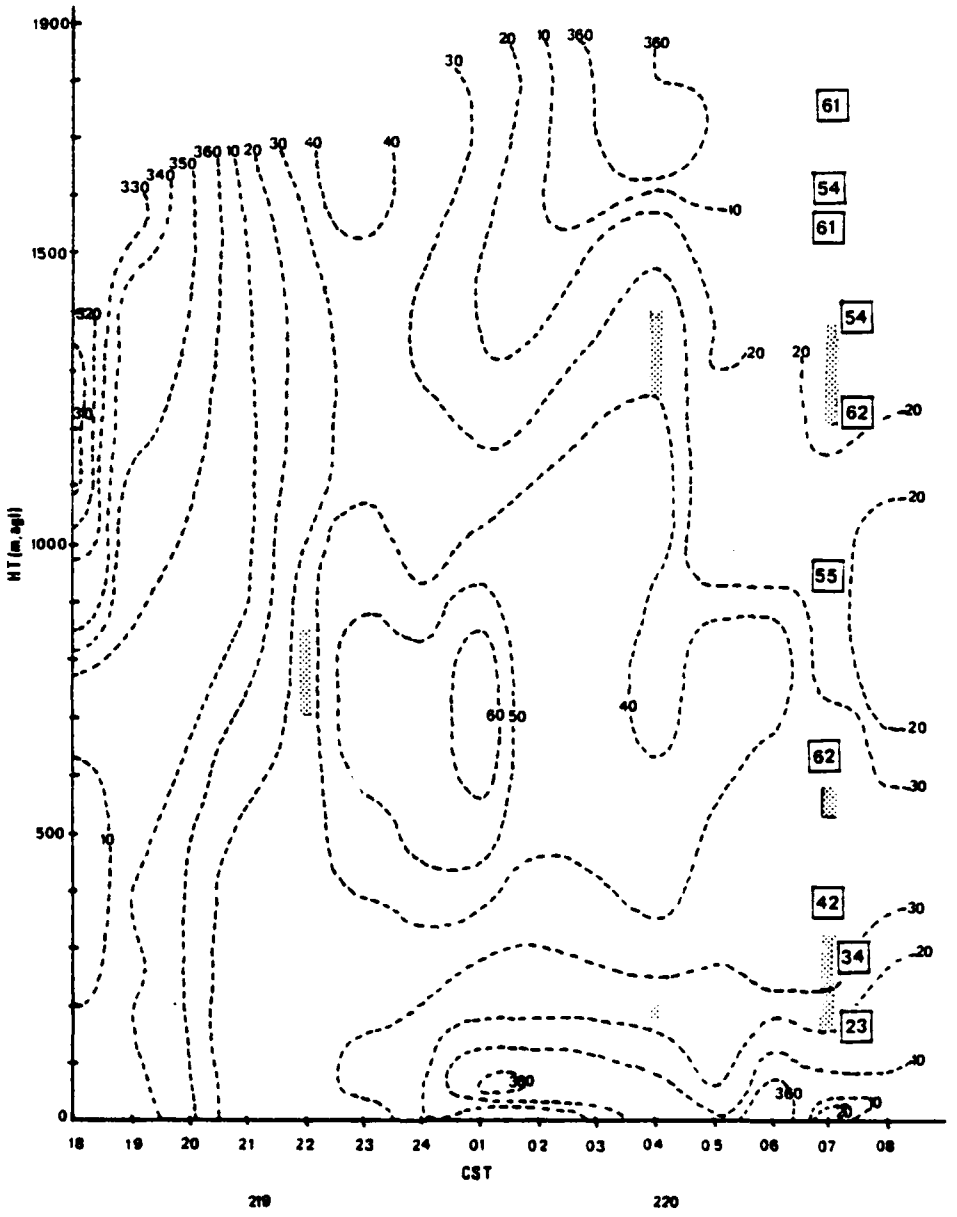


Figure 5.18b Height-time section of wind direction for day 220. Shaded area represents an inversion. Wind direction in degrees. □ indicates ozone concentration in ppb.

Changes in the wind direction for day 220 are shown in Figure 5.18b. Between 1800 and 2200 CST the winds at all levels veered. After 2200 CST the wind direction associated with the relatively large wind speed maximum centered at approximately 700 m AGL remained fairly constant until approximately 0100 CST. As the jet lowered the wind direction in the layer around 700 m AGL showed little change until 0400 CST after which the winds began to back. The winds near the top of the radiation inversion which formed between 2200 CST and 2400 CST showed little or no variation with time during the night.

Figure 5.18a shows the formation of a jet at approximately 1300 m AGL between 1900 and 2000 CST and the subsequent redevelopment of the jet at lower levels prior to the 0600 CST radiosonde launch.

The wind direction (Figure 5.18b) is also variable between radiosonde launch times. The greatest change occurs in the layer associated with the jet whose core was at approximately 700 m AGL. The wind direction changed significantly in the layer above 1000 m AGL between 1800 and 0600 CST. The layer between the top of the radiation inversion and approximately 400 m AGL exhibited little change in direction after approximately 2100 CST.

The 200 m-layer trajectories along with the 12-hour hand computed trajectory are shown in Figure 5.19. The hand computed trajectory and computer produced trajectory lie along the same path. The longer path length for the hand computed trajectory is due to the higher wind speeds that appear in the 200 to 400 m AGL layer as early as approximately 2200 CST. Even though the 19 $m\,s^{-1}$ jet at approximately 0500 CST may not be real, the wind speed height-time section indicates that

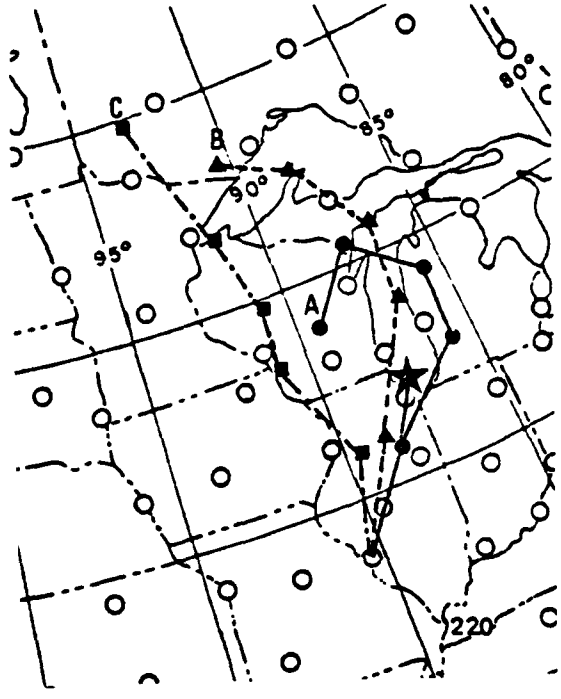


Figure 5.19 200 m-layer average trajectory for day 220. Trajectory A is for 200-400 m AGL layer, Trajectory B is for 900-1100 m AGL layer, and Trajectory C is for 1700-1900 m AGL layer. "★" indicates the end point of the 12-hour hand computed 200-400 m AGL trajectory. Each segment represents 12 hours.

significant speed maxima (11 to 13 $m\,s^{-1}$) existed in the 200 to 400 m AGL layer between 1800 and 0600 CST. The jet centered at approximately 700 m AGL would have also affected the 900 to 1100 m AGL layer trajectory causing the computer to underestimate the path length of the 12-hour segment.

A comparison of Figures 5.17 and 5.19 indicates that the overall trajectory (maximum layer top 2000 m) follows almost the same path as that followed by the 900-1100 m AGL layer trajectory. In Figure 5.19 the three 200 m-layer trajectories define a relatively narrow source region during the first 12-hour segment backward in time from St. Louis. However, between the 12-hour position and the 24-hour position the source region defined by the three 200 m-layer trajectories becomes extremely large.

### 5.4.4 Ozone Profile

Figure 5.20 shows the vertical profile of $O_3$, NO, $NO_x$, and temperature for day 220.

The ozone profile for day 220 is similar to the ideal afternoon profile, Type D (Ludwig, 1979a), except that layers of ozone appear above the mixing height established the previous afternoon.

Figure 5.18b contains a representative sample of the vertical concentration of ozone plotted at the time of the helicopter flight (0707 CST). Either no radiation inversion or only a very shallow inversion has existed during the night. This is a possible explanation as to why the lowest 600 m AGL shows a gradual decrease in ozone from a maximum at 600 m AGL to a minimum at the surface. In this layer (surface to 600 m AGL) no significant increase in $NO_x$ has

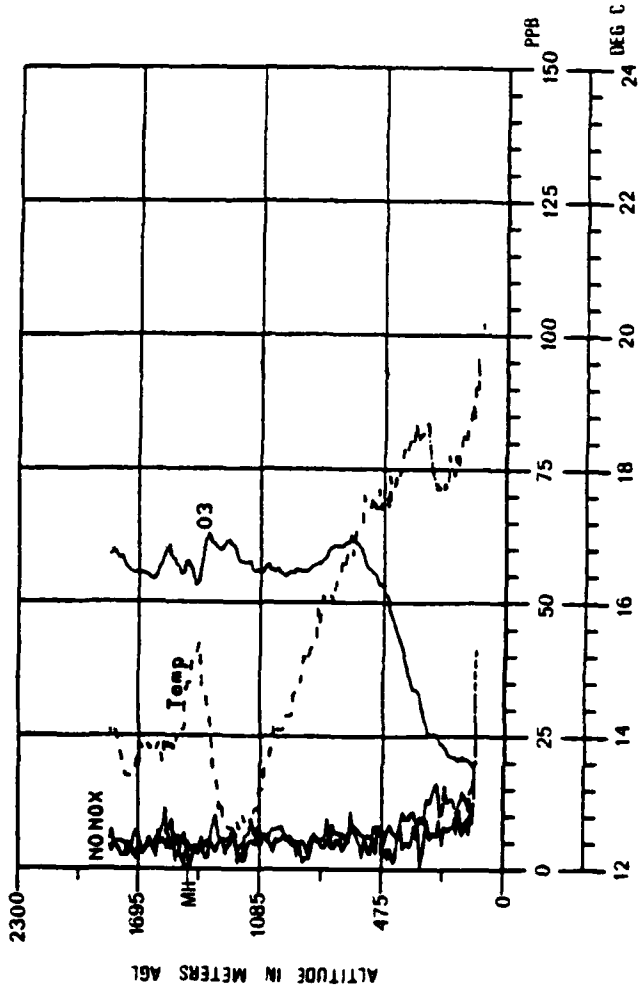


Figure 5.20 Ozone, NO, $NO_x$, and temperature versus altitude, day 220. Upward spiral over Smartt Field between 0707 and 0720 CST. "MH" indicates mixing height on the previous afternoon upwind of Smartt Field.

occurred. Therefore, the scavenging of ozone can be attributed to dry deposition.

Little directional shear occurs in the air above 600 m AGL over Smartt Airfield at the time of the helicopter flight. However, the directional shear that does occur above 400 m AGL between 1800 and 0600 CST is not isolated to a shallow region but, instead, persists almost uniformly throughout the layer from 400 m to approximately 1500 m AGL.

The ozone profile for day 220 shows some layers of ozone above the top of the inversion located between 1300 and 1400 m AGL. The temperature sounding recorded by the helicopter indicates that there are multiple inversions above approximately 1400 m AGL. This stratification, which did not exist in the previous afternoon's upwind sounding, is a possible explanation for the layer of ozone observed above the inversion located between 1200 and 1400 m AGL.

## 5.5 Case V: Day 221

### 5.5.1 Synoptic Chart Discussion

The high pressure center which was near Green Bay on day 220 remains almost stationary at 0600 CST on day 221 (Figure 5.21). The ridge extends south-southeastward across Missouri to the Gulf of Mexico. Due to domination of the ridge over eastern Missouri, the flow at the surface is from the north-northeast.

By 0600 CST on day 221 the dominating feature at 850 mb is the ridge extending from the Great Lakes, through Missouri, to the Gulf of Mexico. This ridge leads to a north-northeasterly flow field over eastern Missouri.

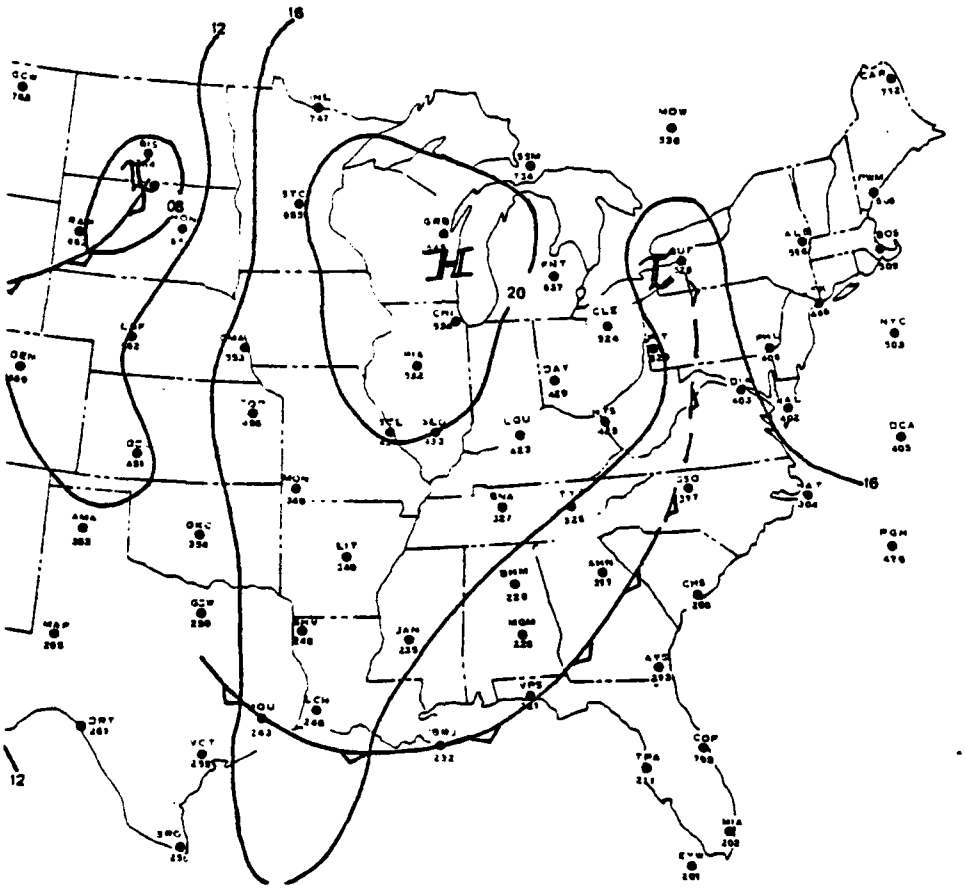


Figure 5.21 Surface analysis for day 221 at 0600 CST

At 700 mb the low has remained stationary while the high has drifted slightly eastward. The flow field over eastern Missouri remains out of the north-northwest with an increase in the magnitude of the winds.

### 5.5.2 Trajectory Analysis

The trajectory for day 221 is shown in Figure 5.22. The trajectory begins north of Lake Superior, moves southeastward to just north of Lake Michigan and then south-southwestward passing near Chicago before arriving over St. Louis.

The 12-hour trajectory segments are nearly uniform with anticyclonic curvature during the first 24 hours and light cyclonic curvature during the last 36 hours.

### 5.5.3 Nocturnal Wind Profile

The height-time sections of wind speed and direction were obtained as described in Case I. The height-time sections for day 221 are shown in Figures 5.23a and b.

Figure 5.23a shows that the radiation inversion and a very pronounced low level jet have formed by 2100 CST. By 0300 CST the low level jet has dissipated and a speed minimum exists between 400 and 700 m AGL with a weak speed maximum occurring near the top of the subsidence inversion. After 0500 CST the wind speed shows little change between the top of the radiation inversion and the base of the subsidence inversion.

Figure 5.23b indicates that in the layer associated with the low level jet the wind direction changes from 020 to 070 degrees between

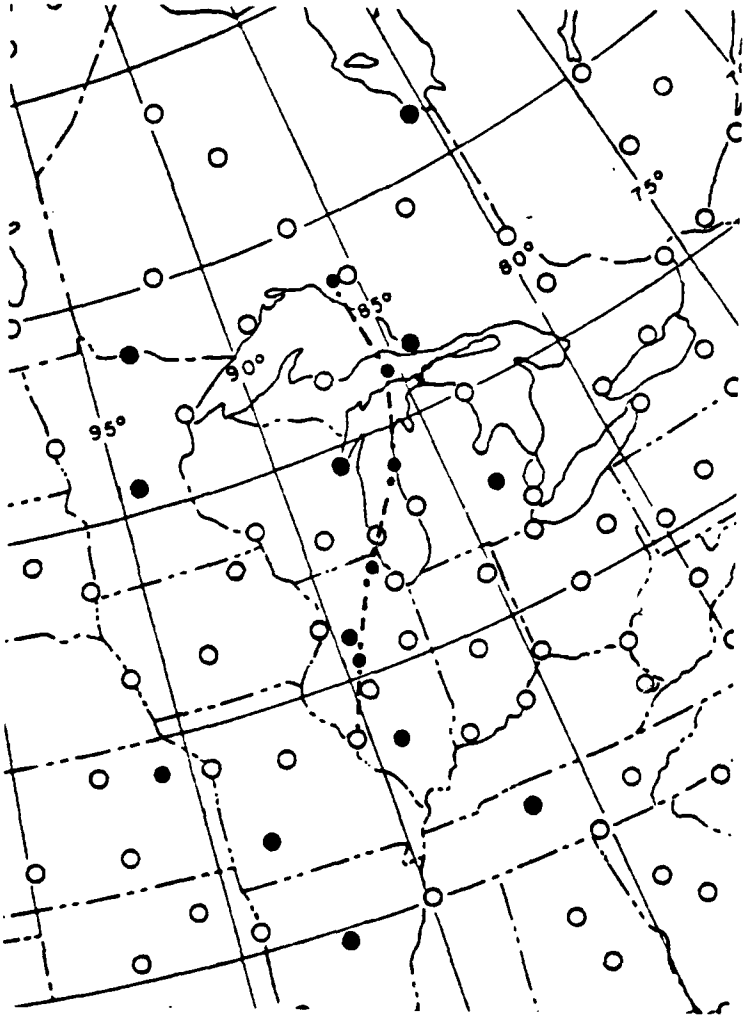


Figure 5.22 Layer-average trajectory for day 221. Maximum top of layer is 2000 m; base of the layer is chosen by the trajectory model. "•" indicates a radiosonde station within 300 nm (approximately 550 km) of trajectory. Each segment represents 12 hours.

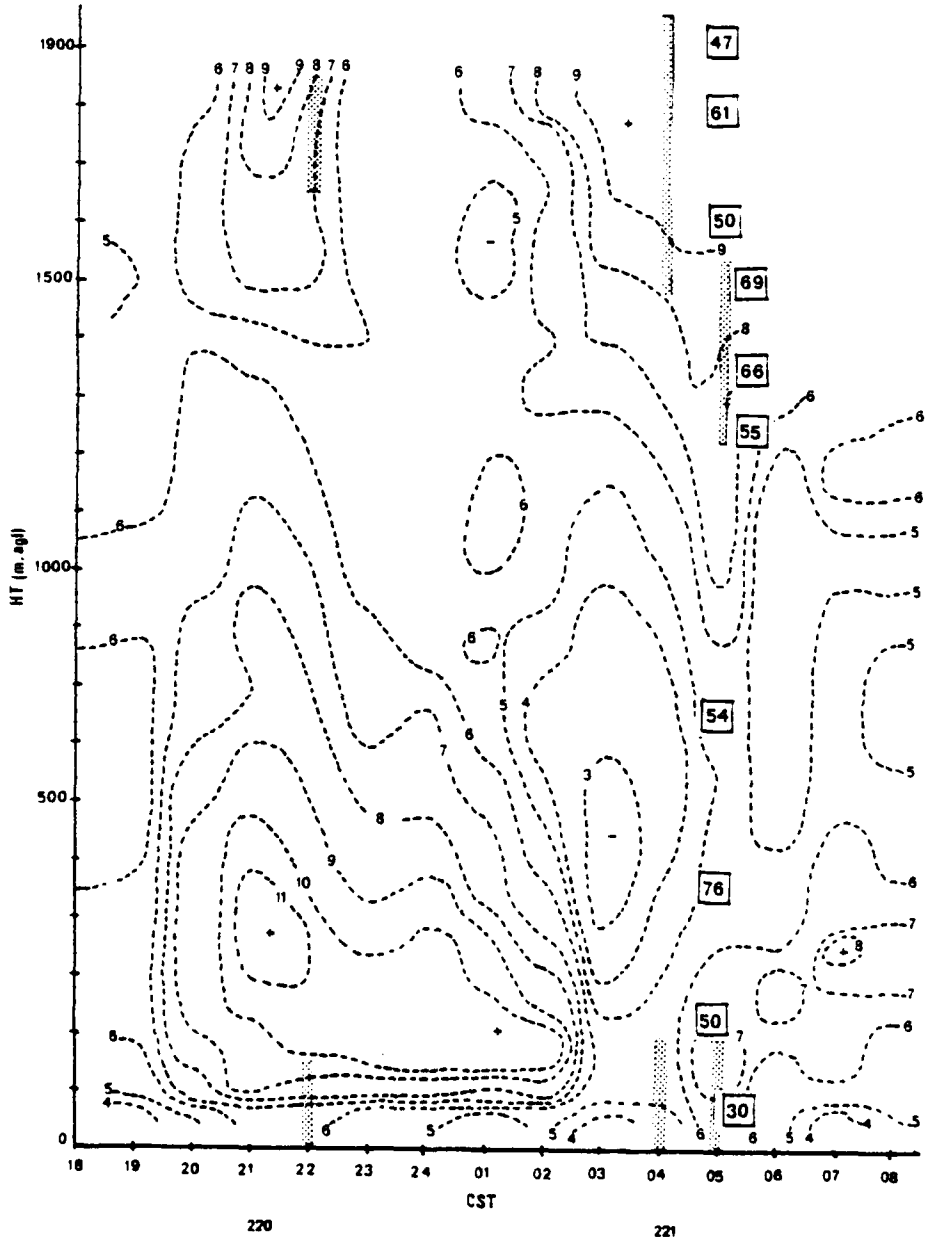


Figure 5.23a Height-time section of wind speed (m $s^{-1}$) for day 221. Shaded area represents an inversion. A "+" indicates a wind speed maximum. A "-" indicates a wind speed minimum. ☐ indicates ozone concentration in ppb.

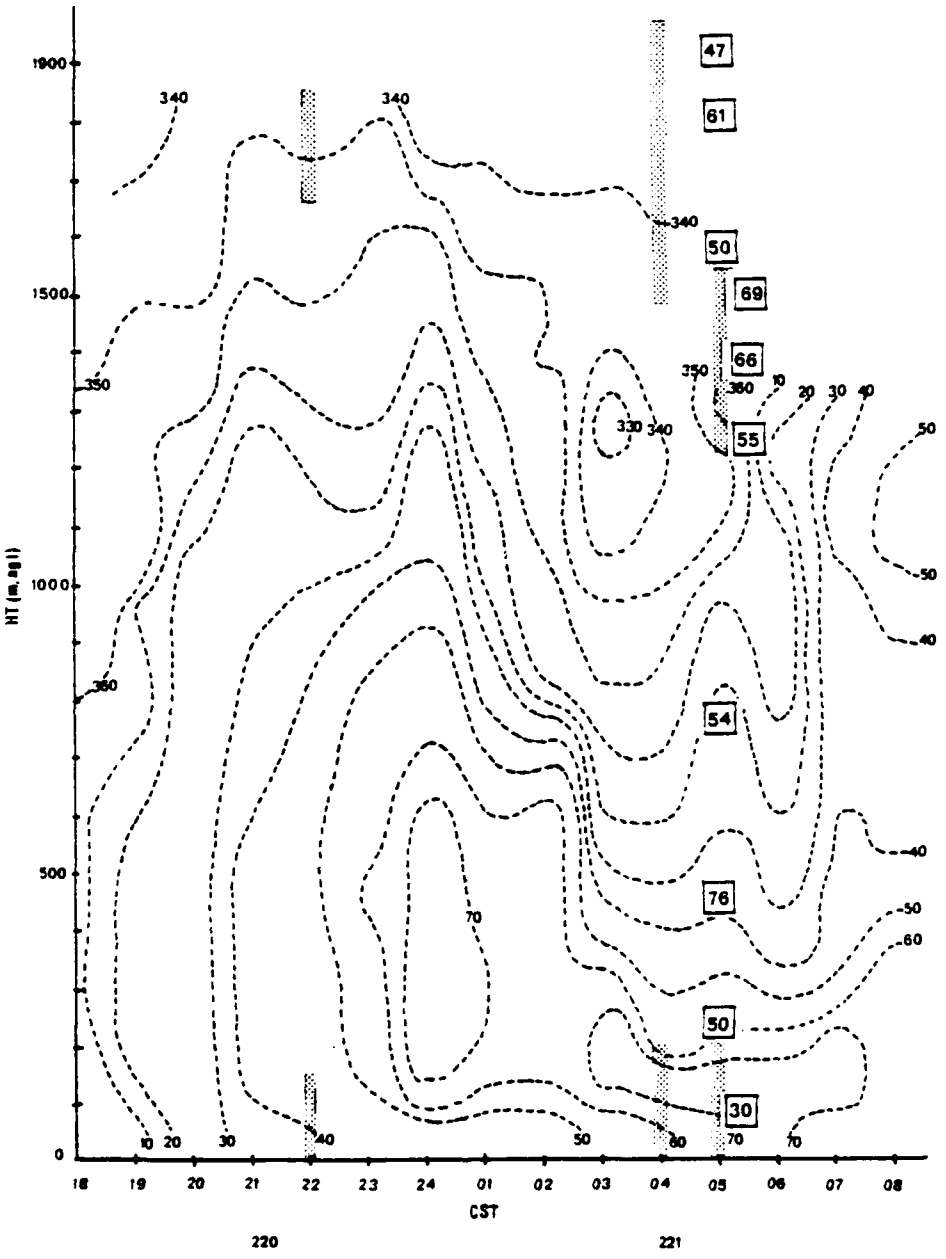


Figure 5.23b Height-time section of wind direction for day 221. Shaded area represents an inversion. Wind direction in degrees. □ indicates ozone concentration in ppb.

1900 and 2400 CST. After 2400 CST a region of maximum shear, which begins at approximately 1400 m AGL, lowers to a lowest point of 200 m by 0400 CST and then increases in height after 0600 CST. The maximum shear zone is associated with the wind speed minimum which occurs at about 0300 CST (Figure 5.23a). Figures 5.23a and b indicate that the dissipation of the jet and the lowering of the shear zone to its lowest point occur almost simultaneously.

Both the jet and the layer of wind shear occur between scheduled radiosonde launches (1800 and 0600 CST). Thus, again the computer produced trajectories will not be totally representative of the changes in the nocturnal wind field.

Figure 5.24 depicts the three 200 m-layer trajectories and the 12-hour hand computed trajectory for the 200 to 400 m AGL layer. The hand computed position for the 200-400 m AGL layer lies to the east of the position computed by the trajectory model and is farther from St. Louis than predicted by the trajectory model. Figure 5.23b also indicates that the 900-1100 m AGL trajectory should possibly lie slightly farther to the east than its computed position with little change in the segment length during the first 12 hours.

A comparison of Figures 5.22 and 5.24 indicates that the overall layer average trajectory follows almost the same path as the 900-1100 m AGL trajectory. Figure 5.24 also shows that the source region expands in the first two segments (24 hours) backward in time from St. Louis.

### 5.5.4 Ozone Profile

Figure 5.25 shows the vertical profile of $O_3$, NO, $NO_x$ and temperature (as described in Case I) for day 221.

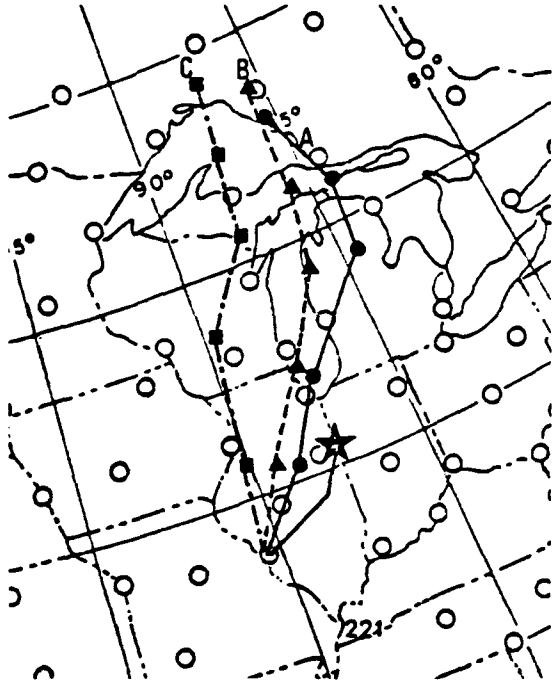


Figure 5.24 200 m-layer average trajectory for day 221. Trajectory A is for 200-400 m AGL layer, Trajectory B is for 900-1100 m AGL layer, and Trajectory C is for 1700-1900 m AGL layer. "★" indicates the end point of the 12-hour hand computed 200-400 m AGL trajectory. Each segment represents 12 hours.

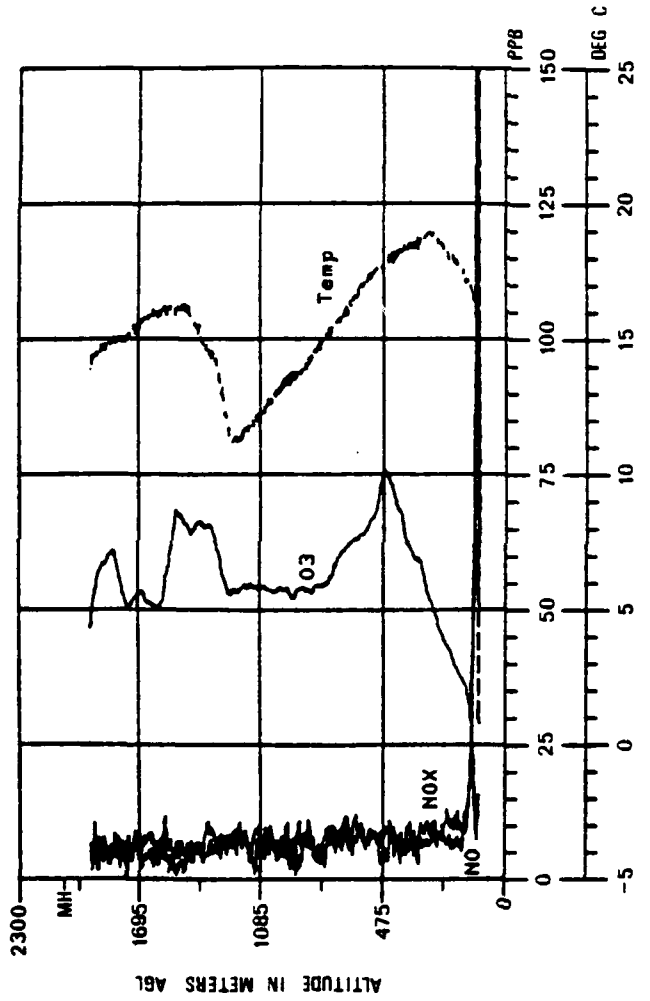


Figure 5.25 Ozone, NO, $NO_x$, and temperature versus altitude, day 221. Upward spiral over Smartt Field between 0437 and 0451 CST. "MH" indicates mixing height on the previous afternoon upwind of Smartt Field.

The ozone profile for day 221 has a sharp "spike" located approximately 250 m above the top of the surface-based radiation inversion. The sharp decrease in ozone occurs well below the mixing height established on the previous afternoon.

Figure 5.23 contains a representative sample of the vertical concentration of ozone plotted at the time of the helicopter flight (0437 CST). In the region above the maximum concentration (76 ppb at 450 m AGL) and below the subsidence inversion the wind direction changes by as much as 60 degrees reflecting the directional shear zone which had gradually lowered during the night. This indicates that the maximum change in ozone concentration is associated with the maximum change in wind direction. Figure 5.23a shows that the maximum concentration of ozone is in a layer where the wind speed is a minimum and at approximately the same height as the nocturnal speed maximum.

The ozone profile for day 221 also indicates a significant layer of ozone within and above the subsidence inversion. The layers of ozone may have been trapped above the subsidence inversion as it lowered during the night.

The ozone profile for day 221 also shows a decrease of 26 ppb from the ozone maximum to the top of the radiation inversion. A subsequent spiral ending at approximately 0450 CST detected an $NO_x$ plume between the top of the radiation inversion and the max observed ozone (76 ppb at 450 m). This would account for the depletion of the ozone above the top of the radiation inversion.

## 5.6 Summary

The height-time sections for each of the five case study days have shown that the nocturnal wind field between the top of the radiation inversion and the base of the subsidence inversion is highly variable. The wind field not only exhibits variability with time but also exhibits a large amount of vertical variability above an observation site at a given time. In addition, the height-time sections have shown that most of the variability in wind speed and direction occurs between the scheduled launch times (1800 CST and 0600 CST) of radiosondes routinely used to obtain wind observations.

The vertical variability of wind direction is most evident on days 216, 217, and 221 (Figure 5.8b, 5.13b, and 5.23b, respectively). On days 215 and 220 (Figures 5.3b and 5.18b) the winds were fairly uniform at the time of the helicopter spiral, but the winds had exhibited changes in direction earlier in the night.

### 5.6.1 Trajectory Analysis

In all five cases the trajectory computed for the original layer (maximum top 2000 m) followed almost the same path as the trajectory for the 900-1100 m AGL layer trajectory. This agreement might be expected since the 900-1100 m AGL layer is approximately in the middle of the original layer (maximum top 2000 m AGL) depending on the top and base of the layer chosen by the trajectory model (the maximum height of the layer base was 500 m AGL).

The 200 m-layer trajectories presented in Figures 5.4, 5.9, 5.14, 5.19, and 5.24 outline the region which could be considered the source

region for the pollutants arriving over Smartt Field. The trajectory for day 215 (Figure 5.4) and day 216 (Figure 5.9) indicated the least variance in the size of the source region for the entire 60-hour trajectory with day 220 (Figure 5.19) indicating the most variance between layers and possibly the largest source region compared to the other case study days.

The Heffter-Taylor Trajectory Model is intended for use as a regional scale trajectory model (Heffter et al., 1975). Therefore, it may not be entirely correct to compare the results of the model to the 12-hour hand computed trajectory, since the hand computed trajectory uses only the winds obtained over one site. However, the comparison is important since it gives an idea of the error that may be present in the first 12-hour segment due to the variability of the nocturnal wind field. The end point of the first segment is the starting point of the second segment; thus, the errors would be cumulative with time.

### 5.6.2 Ozone Profile

The morning ozone profiles for days 216 (Figure 5.10) and 221 (Figure 5.25) have almost the same shape between the top of the radiation inversion and the base of the subsidence inversion. The ozone profiles for both days exhibit a sharp "spike" of ozone above the top of the radiation inversion with uniform ozone concentrations between the point where the ozone concentrations decrease to a minimum (possibly natural background levels) and the base of the subsidence inversion. On day 221 layers of ozone are present above the top of the subsidence inversion as opposed to uniform ozone concentration above the subsidence inversion on day 216.

The height-time sections of wind speed and direction for days 216 (Figures 5.8a and b) and 221 (Figures 5.23a and b) are also very similar. In both cases very pronounced directional shear and a persistent nocturnal jet are present. For days 216 and 221 the height-time cross sections for wind speed indicate that the maximum concentration of ozone occurs in a region where the wind speed is a minimum and at approximately the same height as the jet maximum which occurred during the night. However, by the time of the helicopter spirals the jet had either dissipated (day 221) or was decreasing in magnitude (day 216).

The ozone profile for day 217 (Figure 5.15) exhibits more of a uniform distribution of ozone (if allowances are made for the $NO_x$ plume) between the top of the radiation inversion and the base of the subsidence inversion as compared to the sharp "spike" or ozone observed on days 216 and 221.

The height-time sections for day 217 (Figure 5.13a and b) indicate marked directional shear and a persistent nocturnal jet, as were present on days 216 and 221. In this profile the maximum concentration of ozone occurs within the region of maximum directional shear where the wind speeds are at a minimum and decoupling between the layers probably exists. On day 217 as on days 216 and 221 the ozone maximum occurs in a region of wind speed minimum near the level of the wind speed maximum that occurred during the night. Figures 5.13a and b indicate that at the time of the helicopter spiral the ozone maximum occurs approximately 600 m above the level of the jet maximum and that approximately 150 degrees of directional shear exists between the level of the jet maximum and the maximum ozone concentration. Therefore, the different levels

of ozone present seem to be related more to directional shear than to the wind speeds present.

The ozone profile for day 215 (Figure 5.5) exhibits a uniform distribution of ozone for approximately 500 m above the top of the radiation inversion then decreases fairly rapidly (33 ppb) in the next 500 m layer. Figure 5.3b, which depicts the height-time section of wind direction with a representative sample of the vertical concentration of ozone, indicates that little or no directional shear exist above Smartt Field at the time of the helicopter spiral. A possible explanation for the decrease in the ozone concentration may be the change in the wind direction with time that occurred below 800 m AGL but did not occur above 800 m AGL. The variation of the nocturnal wind field with time may have affected the shape of some portion of the profile prior to its arrival over St. Louis. The path followed by an air parcel prior to arrival over Smartt Field would not be the same for an air parcel below 800 m AGL as compared to an air parcel above 800 m AGL. This could be an indication that the air parcels at different levels have different regions of origin, as on days 216, 221, and 217.

The ozone profile for day 220 (Figure 5.20) appears to have changed very little from the ideal afternoon ozone profile as described by Ludwig (1979a). The distribution of the ozone is almost uniform between the top of the inversion located at approximately 600 m and the base of the subsidence inversion. Though little directional shear exist at the time of the helicopter spiral, wind direction variability has existed during the night as shown in Figure 5.18b. The directional shear which occurred during the night prior to the helicopter spiral on

day 220 occurred almost uniformly from the top of the inversion at approximately 600 m to the base of the subsidence inversion. Therefore, the air in the layer from approximately 600 m to the base of the subsidence inversion appears to have originated from the same source region.

The trajectory analyses, with the exception of day 217, indicate that within 15 to 27 hours before the trajectory arrived over Smartt Field the source region (as described in section 5.6.1) encompassed the major urban-industrial area around southern Lake Michigan. The major urban-industrial area around southern Lake Michigan will be assumed to extend from Milwaukee, Wisconsin, south to the Chicago, Illinois - Gary, Indiana area.

The eastern edge of the source region is uncertain on days 215, 216 and 221 due to the nocturnal variability indicated in the hand computed trajectory. The trajectory analysis for day 217 indicates that the source region encompassed the area around southern Lake Michigan approximately 48 hours prior to the arrival of the trajectories over Smartt Field.

The time of day when the trajectory passes over an urban-industrial area is a primary determinant of the pollutant burden that will be carried away from the area (Ludwig, 1979b; Hester et al., 1977; White et al., 1977). If the trajectory passes over an urban area at night or in the early morning hours (prior to rush hour traffic), the pollutant burden of the trajectory will not be increased as much as it will be if passage occurs between mid-morning and sunset. This is especially true if a radiation inversion is present in the morning

when passage occurs. The term "pollutant burden" refers not only to ozone but also to the precursors from which ozone will form downwind of the urban-industrial area.

Table 5.1 Comparison of the character of the morning profile and the estimated time of trajectory passage over southern Lake Michigan

| Day | Character of Morning Ozone over St. Louis | Estimated Time of Passage over Southern Lake Michigan (CST) |
|---|---|---|
| 216 | Sharp Ozone Spike | 0300 - 0600 |
| 221 | Sharp Ozone Spike | 0300 - 0600 |
| 215 | Uniform Profile | 0900 - 1500 |
| 220 | Uniform Profile | 0900 - 1500 |
| 217 | Uniform Profile | Trajectory Uncertain |

Table 5.1 indicates that the area around southern Lake Michigan is most likely to make a significant contribution to the pollutant burden on days 215 and 220 and least likely to make a significant contribution on days 216 and 221, while the contribution to the pollutant burden on day 217 is uncertain.

A qualitative comparison of the surface synoptic patterns that were present at 0600 CST on the morning the ozone profiles were observed indicates that on days 215 and 220 the gradient of pressure over the St. Louis area was greater than on days 216, 217, and 221.

The height-time sections of the wind field are similar for days 216 and 221 as are the source regions and the times when trajectories intersect the same urban-industrial area. It is not surprising, then,

that the ozone profiles are similar on the two days, even though they are not contiguous. Almost the same applies to days 215 and 220, where the height-time sections, and time of intersection of the urban-industrial area are fairly similar as are the morning ozone profiles for the two days. The height-time section for day 217 is most like days 216 and 221 with the exception that more variability exists in the layer between the top of the radiation inversion and the base of the subsidence inversion, with more stagnant conditions present than on the previous days.

AD-A090 633 AIR FORCE INST OF TECH WRIGHT-PATTERSON AFB OH F/G 4/2
A STUDY OF THE VERTICAL DISTRIBUTION OF OZONE AND THE VARIABILI--ETC(U)
1979 D R HOOD
UNCLASSIFIED AFIT-CI-79-160T NL

2 OF 2

# 6.0 CONCLUSIONS

## 6.1 Trajectory Analysis

The following conclusions can be drawn from analysis of the trajectories and the height-time sections:

(1) The height-time sections of wind speed and direction have shown that the nocturnal wind fields are highly variable with time and that significant changes can occur between scheduled launch times of radiosondes routinely used to obtain wind observations.

(2) Since the radiosonde observations do not detect changes in the nocturnal wind field which occur between scheduled launch times, these changes cannot be reflected in the trajectory computations.

(3) The height-time sections of wind speed and direction also indicate that the wind field exhibits a large amount of vertical variability above an observation point at a given time. The vertical variability of the wind field in a layer can be represented, at least in part, by choosing smaller layers within the original layer and computing trajectories for the smaller layers.

(4) Even with the possibility that vertical motion might be taking place, the choice of several small layers as opposed to one overall layer appears to give a better indication of the source region from which the trajectory may have obtained its pollutant burden.

## 6.2 Ozone Profiles

The shape of the morning ozone profile observed in the case studies is highly variable and is sometimes radically different from the morning

ozone profile predicted by Ludwig (1979a). If the ozone profile at sunset on the previous evening is assumed to be a Type D profile (Ludwig, 1979a), which is described by Ludwig as a profile in which the precursors and the ozone that has formed from them are mixed throughout the boundary layer, then the case studies indicate that the shape of the ozone profile on the following morning could be due to one of or a combination of the following:

(1) The variability of the nocturnal wind field, including the variability of the wind speed and direction, and including both the variability with time and vertical variability above an observation point.

(2) The transport of air parcels containing different pollutant burdens in different layers, with little mixing occurring between the layers, over Smartt Field at the time of the helicopter spiral.

(3) The transport of air parcels containing different pollutant burdens by the nocturnal jet.

(4) The proximity of the source region to major urban-industrial areas and the time of day when the trajectory passes the source region.

(5) The formation of and the change in height of both nocturnal radiation inversions and the more persistent subsidence inversions. These changes could also affect the nocturnal wind field.

(6) The natural background levels present in the trajectory air mass. This would determine the minimum levels of ozone that could be observed if the air came from "clean" remote areas.

The case studies indicate that the most plausible explanation for the shape of the ozone profile observed, over Smartt Field at the time

of the helicopter spiral, in the five cases is the transport of air containing different pollutant burdens in different layers, with little mixing occurring between the layers. However, a major problem with the case studies has been a lack of knowledge of the shape of the ozone profile at sunset on the evening prior to the observation of the ozone profile and the changes that occurred in the profile moving with the trajectory prior to the arrival of the trajectory over Smartt Field. Due to the variability of the nocturnal wind field, it does not seem that this problem can be solved easily. Therefore, the best approach to follow would be to observe hourly profiles of ozone, NO, $NO_x$, and temperature in conjunction with hourly wind observations over a chosen point to determine the changes which are taking place in each of the quantities and the possible relationship between the changes.

# LIST OF REFERENCES

Blackadar, A. K. 1957. Boundary layer wind maxima and their significance for the growth of nocturnal inversions. Bulletin American Meteorological Society, 38(5):283-290.

Chatfield, R. and R. A. Rasmussen. 1977. An assessment of the continental lower tropospheric ozone budget. International Conference on Photochemical Oxidant and Its Control, Proceedings. Volume I, EPA-600/3-77-001a, p. 121. U.S. Environmental Protection Agency, Research Triangle Park, N.C., January 1977.

Coventry, D. M. 1979. Private Communication.

Galbally, I. 1968. Some measurements of ozone variation and destruction in the atmospheric surface layer. Nature, 218:456-457.

_____. 1971. Ozone profiles and ozone fluxes in the atmospheric surface layer. Quarterly Journal of the Royal Meteorological Society, 97:18-29.

Garland, J. A. and R. G. Derwent. 1979. Destruction at the ground and the diurnal cycle of concentration of ozone and other gases. Quarterly Journal of the Royal Meteorological Society, 105:169-183.

Harrison, R. M., C. D. Holman, H. A. McCartney, and J. F. R. McIlveen. 1978. Nocturnal depletion of photochemical ozone at a rural site. Atmospheric Environment, 12:2021-2026.

Heffter, J. L., A. D. Taylor, and G. J. Ferber. 1975. A regional-continental scale transport, diffusion and deposition model. NOAA TM ERL ARL-50, 29 pp., Silver Springs, Maryland, pp. 1-16.

Hester, N. E., R. B. Evans, F. G. Johnson, and E. L. Martinez. 1977. Airborne measurements of primary and secondary pollutant concentrations in the St. Louis urban plume. International Conference on Photochemical Oxidant and Its Control, Proceedings. Volume I, EPA-600/3-77-001a, p. 259, U.S. EPA, Research Triangle Park, N.C., January 1977.

Hoecker, W. H. 1977. Accuracy of various techniques for estimating boundary-layer trajectories. Journal of Applied Meteorology, 16: 374-383.

Ludwig, F. L., E. Reiter, E. Shelar, and W. B. Johnson. 1977. The relation of oxidant levels to precursor emissions and meteorological features. Volume I. Analysis and Findings, EPA-450/3-77-022a, EPA, OAQPS, Research Triangle Park, N.C., October 1977.

_____. 1979a. Vertical profiles of photochemical pollutants in the vicinity of several urban areas. Proceedings Fourth Symposium Turbulence, Diffusion and Air Pollution, Reno, Nevada, 15-18 January 1979 (American Meteorological Society, Boston, Massachusetts).

_____. 1979b. Assessment of vertical distributions of photochemical pollutants and meteorological variables in the vicinity of urban areas. Draft final report for SRI Project No. 6869, January 1979.

Mage, D. T., R. B. Evans, C. K. Fitzsimmons, N. E. Hester, F. Johnson, S. Pierett, G. W. Siple, and R. N. Snelling. The RAPS helicopter air pollution measurement program, St. Louis, Missouri, 1974-1976 (draft). Environmental Monitoring and Support Laboratory, Las Vegas, Nevada.

Ripperton, L. A. and F. M. Vukovich. 1971. Gas phase destruction of tropospheric ozone. Journal of Geophysical Research, 76(30:7328-7333.

Singh, H. B., F. L. Ludwig, and W. B. Johnson. 1978. Tropospheric ozone: concentrations and variabilities in clean remote atmospheres. Atmospheric Environment, 12:2185-2196.

Vukovich, F. M. 1973. Some observations of the variations of ozone concentrations at night in the North Carolina Piedmont boundary layer. Journal of Geophysical Research, 78(21):4458-4462.

Wark, K. and C. F. Warner. 1976. Air Pollution, Its Origin and Control. Dun-Donnelley, 503 pp.

White, W. H., D. L. Blumenthal, J. A. Anderson, R. B. Husar, and W. E. Wilson, Jr. 1977. Ozone formation in the St. Louis urban plume. International Conference on Photochemical Oxidant and Its Control, Proceedings. Volume I, EPA-600/3-77-001a, p. 237, U.S. EPA, Research Triangle Park, N.C., January 1977.